Australian Government
Department of Defence
Defence Science and
Technology Organisation

Investigation of Stress Intensity Factor for Overloaded Holes and Cold-Expanded Holes

Richard Callinan, Robert Kaye and Manfred Heller

Air Vehicles Division
Defence Science and Technology Organisation

DSTO-TR-2737

ABSTRACT

For life assessment of airframe components, it is important to understand how the residual stresses due to material yielding affect crack initiation or crack growth at holes. A key step in understanding such effects is the quantification of the Mode 1 stress intensity factor for cracks that may initiate subsequent to overloading. Here, a two-dimensional weight function approach is used to determine stress intensity factors for cracks in either tensile or compressive stress fields due to one of three mechanisms: remote tension overload, remote compression overload or hole cold expansion. The effect of subsequent remote loading is also considered. The key input is the stress distribution in the corresponding uncracked body along the prospective crack path. The key trends are investigated through many numerical examples for symmetrically-cracked holes in large steel and/or aluminium alloy plates. Cold expansion of finite-width plates representative of C-130 wing skin locations is also studied. For both remote overload cases, it is shown that, once the crack length is the same or larger than the initial yield zone, the stress intensity factors are the same as for the case without the initial overload. However, for cold-expanded holes, the beneficial reduction in stress intensity factor extends beyond the initial yield zone. Hence, the present work provides a greater depth of understanding of how typical residual stresses can affect key inputs into airframe life assessment.

RELEASE LIMITATION

Approved for public release

Published by

Air Vehicles Division
DSTO Defence Science and Technology Organisation
506 Lorimer St
Fishermans Bend, Victoria 3207 Australia

Telephone: (03) 9626 7000
Fax: (03) 9626 7999

AR-015-380
July 2012

APPROVED FOR PUBLIC RELEASE

Investigation of Stress Intensity Factor for Overloaded Holes and Cold-Expanded Holes

Executive Summary

Significant work undertaken in Air Vehicles Division involves providing advice on through-life support of Australian Defence Force aircraft. For accurate life assessment of airframe components, it is important to have an understanding of how the residual stresses due to material yielding affect crack initiation or crack growth at holes in metallic components. A key step in understanding such effects is the quantification of the Mode 1 stress intensity factor, for cracks which may initiate subsequent to the overloading. The weight function method is a useful approach to determine Mode 1 stress intensity factors, since the crack does not need to be explicitly modelled. Hence, in the present investigation, a two-dimensional weight function approach is used to determine stress intensity factors for cracks in either tensile or compressive stress fields, due to one of three mechanisms: remote tension overload, remote compression overload or hole cold expansion. An important analysis input is the stress distribution in the corresponding uncracked body along the prospective crack path, obtained from either finite element analysis or theoretical methods.

In the present work, analyses are undertaken to consider key trends and limitations of current prediction methods, with an emphasis on the use of weight function methods. The main areas addressed are as follows. Initially, a detailed literature survey is presented on the use of weight function approaches in the context of three key types of overloads: remote tensile overload, remote compressive overload and local cold expansion. As an example for the generation of stresses along the prospective crack path, finite element analysis of an uncracked hole in a remotely-loaded steel plate is given. Stress intensity factor results for three sets of numerical test cases are then determined. Two of these involve cold-expanded holes in large D6ac steel plates and large aluminium alloy plates. The third test case geometry corresponds to a fatigue test coupon consisting of a finite-width aluminium alloy plate, which is representative of locations on the lower wing skin of the C-130 aircraft. Finally, results and comparison of generic cases for a D6ac steel plate for all three overload cases are given.

For both remote overload cases, it is shown that, once the crack length is the same or larger than the initial yield zone, the stress intensity factors are the same as for the case without the initial overload. However, for cold-expanded holes, the beneficial reduction in stress intensity factor extends beyond the initial yield zone. A set of Fortran computer programs has been written to generate the results in this report. These programs are given on an enclosed Compact Disc for future reference and use. The present work has provided a greater depth of understanding of how typical residual stresses can affect key inputs into airframe life assessment. The use of these techniques can assist in providing more timely and accurate prediction of fatigue life, for Australian Defence Force platforms.

This page is intentionally blank

Authors

Richard Callinan
Air Vehicles Division

Mr Richard Callinan is a Senior Research Scientist and graduated from RMIT (Aero Eng) in 1969 and from Monash University in 1971 (Civil Eng) and completed a MEngSci in 1981 at Melbourne University. His work has been in the areas of finite element analysis, fracture mechanics and structural mechanics of composite and bonded repairs and military aircraft accident investigations. He has also been involved with design studies of low radar cross-section battlefield surveillance UAVs. In 1985 he was seconded to the USAF at Eglin AFB for 18 months, to carry out vulnerability studies on composite structures. More recently he has been involved in a specific program on validation of bonded repairs to RAAF aircraft, and bonded repairs to structures subject to acoustic fatigue. He has over 120 publications, including three book chapters on repair of cracked aircraft structures.

Robert Kaye
Air Vehicles Division

Mr Robert Kaye joined DSTO in 1990 as a structural engineer with a background in naval ship construction and full-scale testing of civil structures. The first three years at DSTO were spent in evaluation of bonded repairs primarily using finite element methods. Included in this was the analysis of repairs to fuselage skin lap-joints, wing planks and bulkhead frames. More recently he has been involved with structural and mechanical aspects of complex full scale fatigue test installations and structural shape optimisation, also using finite element methods.

Manfred Heller
Air Vehicles Division

Dr Manfred Heller completed a BEng (Hons) in Aeronautical Engineering at the University of New South Wales in 1981. He commenced employment in Structures Division at the Aeronautical Research Laboratory in 1982. He was awarded a Department of Defence Postgraduate Scholarship in 1986, completing a PhD at Melbourne University in 1989. He is currently a Principal Research Scientist and Functional Head for Structural Mechanics in Air Vehicles Division, of the Defence Science and Technology Organisation. Since 1992 he has led tasks which develop and evaluate techniques for extending the fatigue life of ADF aircraft components. His research contributions have focussed on the areas of structural shape optimisation, computational and experimental stress analysis, and bonded repair technology. He is a Corresponding Member, on the Committee of Stress Analysis and Strength of Components, Engineering Science Data Units (ESDU) UK.

Contents

Nomenclature

a	normalised crack length, A/R
A	crack length
d_n	coefficient in expression for finite-width stress
D_{PZ}	depth of plastic zone
e_n	coefficient in expression for finite-width stress
E	Young's modulus for plate
E_M	Young's modulus for mandrel
E_P	post-yield modulus in the plastic range
f	nondimensional stress intensity factor
K_I	stress intensity factor
l_n	coefficient in expression for finite-width stress
M	distance ahead of crack tip along prospective crack path
m_n	coefficient in expression for finite-width stress
m	normalised distance ahead of crack tip, M/A
$m(x,a)$	weight function
R	hole radius
R_m	radius of mandrel
S_i	area under the weight function
S_i^*	area under stress function
w	dimension of finite plate
W	characteristic distance
x	normalised distance from hole edge along prospective crack path, X/R

X	distance from hole edge along prospective crack path
X_i	function of coordinate increments and stress function
X_i^*	centroid of stress function
β	weight function coefficient
η	nondimensional re-yield radius
γ	yield criterion
λ	interference level
ρ	nondimensional plastic zone size, D_{PZ}/R
σ_r	remote stress
σ_{ini}	initial overload stress
σ_{max}	peak residual hoop stress at hole boundary
σ_R	radial stress at cold-worked hole
σ_T	tangential stress at cold-worked hole
σ_{vm}	von Mises stress
σ_{xx}	stress in *x* direction
σ_y	yield stress
σ_{yy}	stress in *y* direction
σ_{YYre}	stress in neighbourhood of hole due to remote stress
σ_{YYrs}	residual stress in neighbourhood of hole

1. Introduction

Holes are the most common stress concentration feature in metallic aircraft structures; hence the growth of fatigue cracks at holes is a common occurrence. Overloads at holes can occur due to large service loads experienced by airframe components. These loads can be tensile or compressive, and may result in material yielding at the hole edge. Compressive overloads may more commonly occur on upper wing surfaces while tensile overloads typically occur on lower wing surfaces. A tension overload causes local yielding, followed by unloading, can provide beneficial compressive residual stresses at the hole edge. Conversely, compressive overloads followed by unloading can lead to potentially detrimental tensile residual stresses. Holes can also be overloaded locally to enhance fatigue life. For example, cold working of holes is a technique that is widely used in aircraft structures to induce beneficial compressive residual stresses around the hole. This is achieved using a mandrel drawn through the starting hole in order to apply radial pressure to the hole surface, causing local yielding and material elongation in the circumferential direction.

For the life assessment of airframe components, an understanding of how the residual stresses and initial yield zone affect crack initiation or crack growth is important. A typical step in understanding such effects is the quantification of the Mode 1 stress intensity factor, K_I, for cracks which may initiate subsequent to the overloading. It is desirable to have available some knowledge, even trends, of the following: (i) conditions for which overload effects are significant; (ii) how significant the effects are for different cases, for example, how the effects due to remote overloads compare to local treatments such as cold expansion; and (iii) the accuracy and/or limitations of common analysis approaches for predicting K_I. Based on a review of the literature, it appears that only limited work has been conducted to address these issues. It is also clear that most relevant work has focussed on cold expansion of holes, and on the application of weight function methods to holes or other crack configurations.

Hence, in the present work, analyses are undertaken to consider key trends and limitations of current prediction methods, with an emphasis on the use of weight function methods. A detailed literature survey is presented in Section 2, covering the use of weight function approaches in the context of three key types of overloads: remote tensile overload, remote compressive overload and local cold expansion. The general plate geometry and loading arrangement used in the computational analyses are given in Section 3. The finite element analysis (FEA) of an uncracked hole in a remotely loaded plate is presented in Section 4. In Section 5, the weight function approach is given for cases of a hole in a remotely-loaded plate, as well as for a cold-expanded hole. Section 6 then gives the stress intensity factor results for three sets of numerical test cases. Two of these involve cold-expanded holes in large D6ac steel plates and large aluminium alloy plates. The third test case geometry corresponds to a fatigue test coupon consisting of a finite-width aluminium alloy plate, which is representative of locations on the lower wing skin of the C-130 aircraft. Then Sections 7, 8 and 9 give the results and comparison of generic cases for a D6ac steel plate for all three overload cases. Here, Section 9 focusses on a comparison of results for the cold-expanded hole and the tension-overload case. The conclusions are then given in Section 10. A Compact Disc containing source code for the numerical integration and the examples is provided with this report.

2. Literature survey

Weight function techniques for estimating K_I were first conceived by Bueckner [1]. Rice [2] also obtained the same equation by a different method and demonstrated that the weight function is a universal function. The method is very general, since estimating K_I depends only on the integration of the weight function and the stress distribution along the prospective crack path in the corresponding uncracked body.

2.1 Weight functions and their application

A large number of weight functions have been determined for different conditions, such as cracks emanating from holes, cracks subject to non-uniform stress fields and cold working of holes containing cracks (see for example Wu and Carlsson [3]). Some further examples are as follows. Kiciak et al [4] have derived weight functions for corner-elliptical cracks in a finite-thickness plate. Chen and Wang [5] have derived weight functions for cracks subject to non-uniform stress fields and cold working of holes containing cracks. Glinka and Shen [6] have derived weight functions for edge cracks in infinite plates and through cracks in infinite plates. Mawatari and Nelson [7] have used Gauss–Chebyshev integration in order to eliminate the singularity and reduce the error below 1%. Similarly, Daniewicz [8] has used the same method and has achieved increased computational efficiency. Grandt and Kullgren [9] have tabulated stress intensity factors for flawed fastener holes using a weight function technique. Paris et al [10] have derived weight functions for a number of two-dimensional (2D) problems. Shen and Glinka [11] have derived weight functions for 2D surface semi-elliptical cracks in three-dimensional (3D) plates. Petroski and Achenbach [12] have computed the weight function from stress intensity factors for a reference loading configuration. They obtained crack face displacements that were in good agreement with analytical results for a number of cases, and their technique involves simple quadrature and is very efficient. Sobczyk and Trębicki [13] looked at the effect of random residual stresses on fatigue crack growth and used the weight function technique. A stochastic fatigue crack growth equation was also used to determine the random number of cycles to failure. Jones et al [14] have proposed weight functions for 2D and semi-elliptical cracks emanating from a notch, which are applicable for both short and long cracks. Zhao and Wu [15] have evaluated stress intensity factors for a semi-elliptical surface crack in a semi-circular notch by use of the weight function technique for loads applied on the crack face and the edge of the specimen. Good results are obtained in comparison to FEA. Work undertaken by Roy and Saha [16] involved the development of an analytical expression for the weight function of an elliptical crack under normal loading, and the solution is verified for three separate cases.

2.2 Cold expansion

For the case of plates with cold-worked holes subject to remote loading, Pinho et al [17] have used 2D analytical and semi-analytical methods to predict stress intensity factors. Here a focus was the study of loading conditions and yield zone size required to open the crack fully for Al 2024 Alclad aluminium alloy material. Clark [18] has used the weight function technique to calculate residual stress. Here comparisons with experimental results have shown that the

method can give reasonable predictions of critical crack length. Pavier et al [19] have used 2D and 3D FEA and 2D weight functions to investigate cold expansion of cracked holes. Normalised results are given showing that the weight function technique underestimates the stress intensity factor. The agreement improves with increasing crack length and when the remote loads are high compared to the material yield point. Moreira et al [20] have used both FEA and the weight function technique to determine residual stress intensity for cracked cold-expanded holes (i.e. with no subsequent remote loading) under plane stress conditions. Here good agreement between both methods for a range of crack sizes was shown.

2.3 Compressive overloads

Very few references exist on the effects of compressive overloads applied to plates with open holes. However, heat treatment on 1080 steel has been used to induce tensile residual stresses in a notch in a compact tension specimen by Prawoto [21]. The predictions of stress intensity based on linear elastic fracture mechanics and weight functions compared well with the experimental results.

2.4 Tensile overloads

In the case of tension overloads for plates with open holes, some references do exist. An experimental study has been carried out by Wahab et al [22]. It was found that tensile overloads retard the crack growth rate for a period of time. However, when the crack grows out of the plastic zone the crack growth is no longer retarded. Similarly, the residual stresses considered by Wang [23] are tensile in the plate, and fatigue crack growth is promoted when the crack grows into the residual stress field. Also, for the tension overload case LaRue and Daniewicz [24] have used an elastic–plastic FEA to relatively accurately predict fatigue crack growth using a weight function computation. From references [19, 20, 21], there appears to be some inconsistency in the claimed effectiveness of weight function methods to predict the stress intensity factor when the crack is in a local compressive residual stress field. Work carried out by Yu and Abel [25] has developed a weight function technique capable of predicting stress intensity during partial crack closure. This involves computing the crack surface displacement and a trial-and-error method to calculate K_I, and is applied to a centre-cracked plate. The method is fairly general and may be an option for application to cracking at holes.

3. Geometry and loading arrangement

In this section, the geometry and notation for the two general cases considered are given as follows: (i) overload due to remote loading of a plate containing a central hole and (ii) overload due to cold expansion of a centrally-located hole in a plate. In both cases subsequent elastic remote loading can be introduced.

3.1 Remotely-loaded plate with hole

A 1 mm thick plate of width 2*w* and height 2*h* containing a central hole of radius *R* is shown in Figure 1. The plate is subject to an initial remote load σ_r which may be compressive or tensile. Unless noted otherwise, all analyses are for a large plate, typically with *w* = 10*R*.

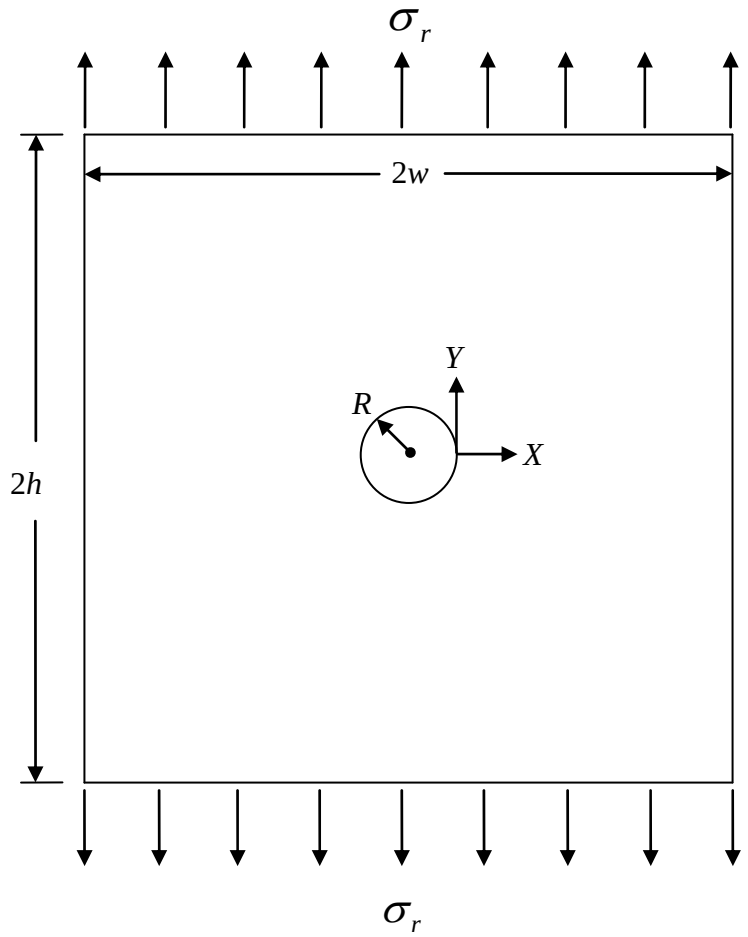

Figure 1: Plate with central hole loaded by remote stress

3.2 Cold-expanded hole

The cold-expanded hole is idealised as shown Figure 2. Once again, the plate width is given as *w*, and here the plate is considered infinitely long. The interference level is defined by:

$$\lambda = \frac{R_M - R}{R} \tag{1}$$

where R_M is the initial radius of the mandrel and R is the initial radius of the hole.

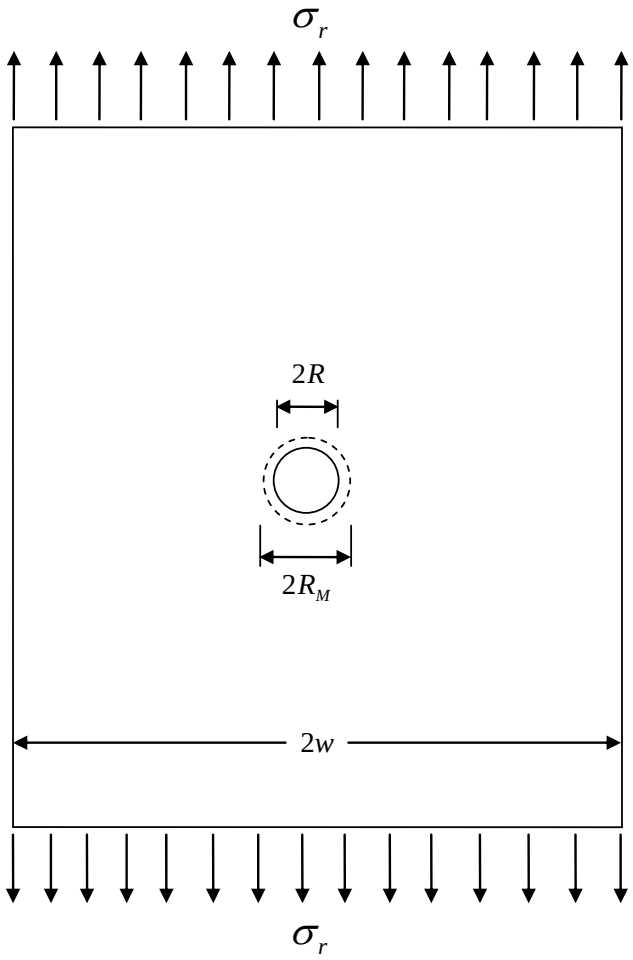

Figure 2: Cold-expanded hole in an infinitely-long plate of finite width subjected to remote stress

4. FEA for uncracked hole in remotely-loaded steel plate

The following sub-sections cover the finite element mesh, modelling parameters, boundary conditions and typical stress results due to compressive and tensile overloads. Some results corresponding to the subsequent application of a tensile service load are also given. The analysis is two-dimensional with plane stress conditions being assumed unless otherwise stated. The ABAQUS version 6.9 structural analysis software code is used for the FEA. Unless noted otherwise, all analyses represent a large D6ac steel plate. These stress results are then used in Sections 7 and 8 to determine stress intensity factors using the weight function method for tensile and compressive overload cases respectively.

4.1 Finite element mesh and material modelling parameters

4.1.1 Mesh and elements

Consider a uniaxially-loaded square plate with a central hole as shown in Figure 3, which leads to the development of regions of plastic flow as shown in Figure 4. The finite element model assumes ¼ symmetry. As shown in Figures 5 and 6, the region along the prospective crack path has a highly-refined mesh consisting of 4-noded quadrilateral elements. Each element has an edge length of 0.01 mm compared with the hole diameter of 10 mm. Three-noded triangular elements have been used for the transitioning of the mesh and the remainder of the ¼ model.

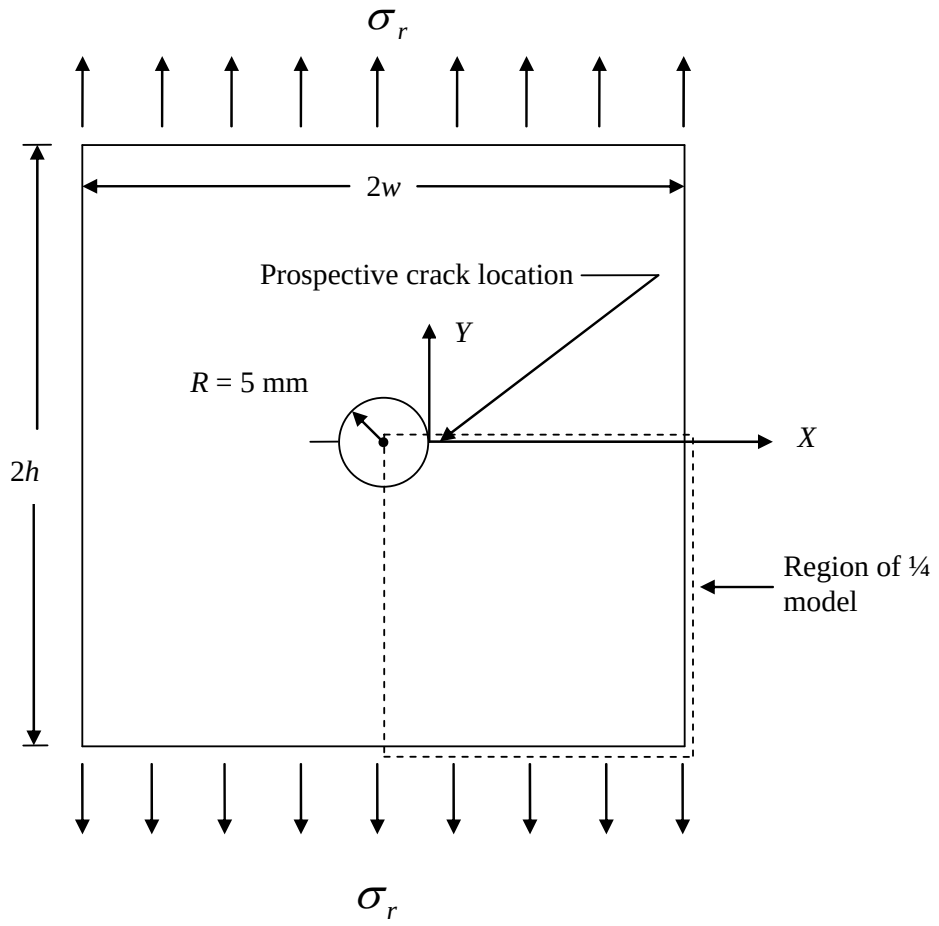

Figure 3: Geometry for finite element model showing prospective crack location

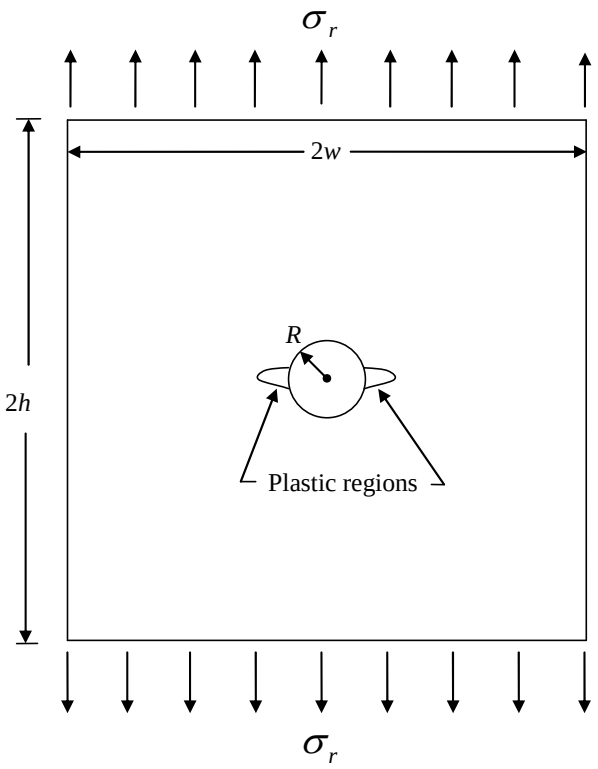

Figure 4: Geometry showing expected plastic regions

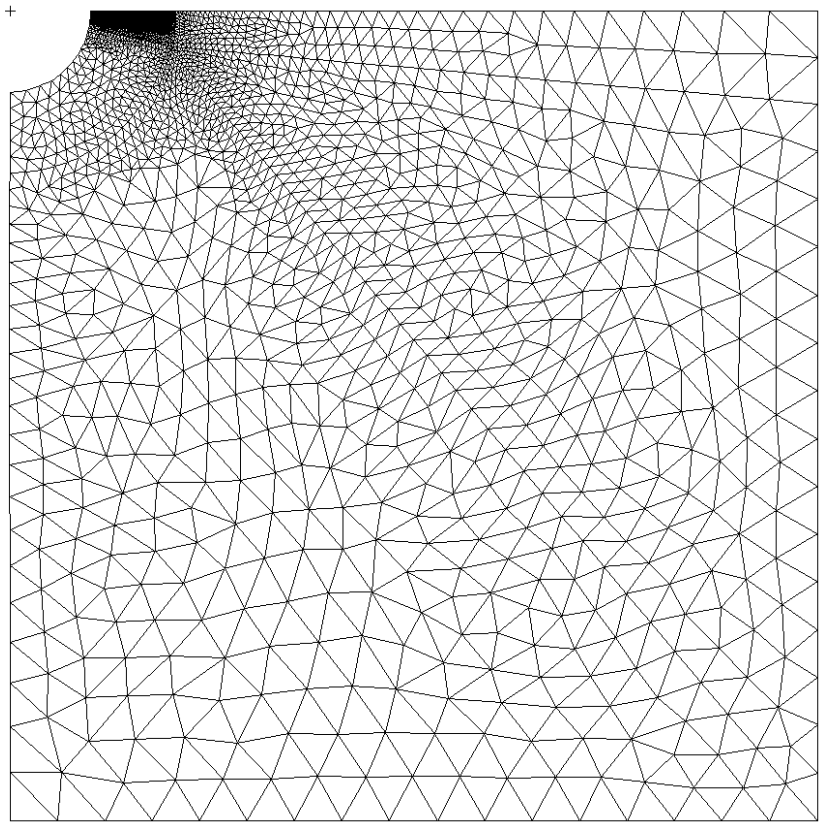

Figure 5: Mesh of quarter model showing dense region at crack site

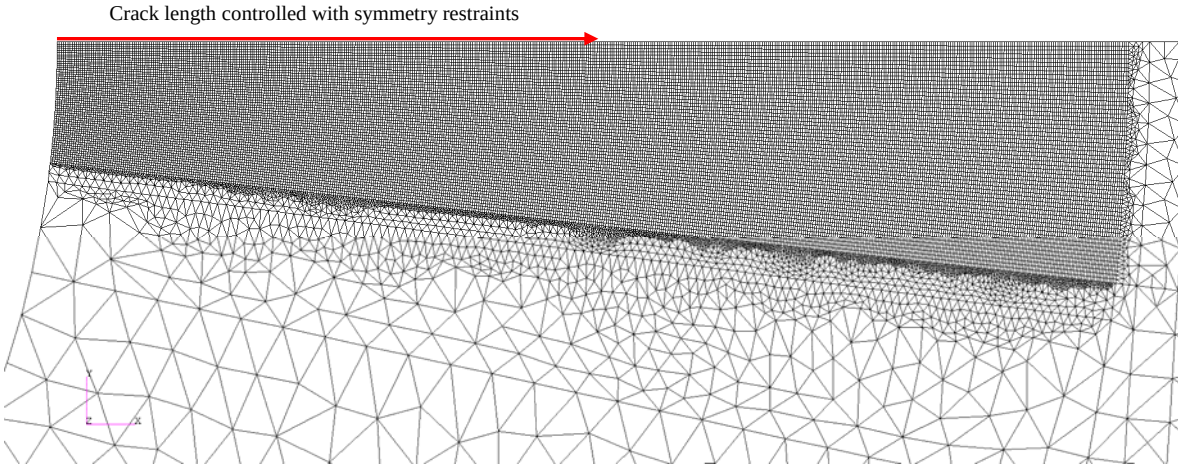

Figure 6: Mesh in crack-site region

4.1.2 Material

The analysis is materially nonlinear and the von Mises yield criterion is used. The material used is D6ac steel and the properties are given in Table 1 (see [26]).

Table 1: Material properties for constitutive model for D6ac steel

E (MPa)	σ_Y (MPa)	E_P (MPa)
200,000	1,309	1,824

In the above Table, E is the Young's Modulus, σ_Y is the yield stress, and E_P is the modulus in the plastic range. It can be seen that the response is close to elastic–perfectly plastic.

4.1.3 Boundary conditions

Displacement constraints due to symmetry are applied in the X direction along the left-hand boundary at $X = -R$, as shown in Figure 5. Similarly, displacement constraints are also applied in the Y direction along the top boundary at $Y = 0$ in Figure 5.

4.1.4 Loading and nonlinear convergence

The ABAQUS code automatically selects the number of load steps to be used in the analysis to achieve a selected convergence criterion. Here, for an increment of load, the sum of the internal nodal forces is compared to the total applied load. The criterion chosen is that for an acceptable solution this difference is less than 0.5%.

4.1.5 Mesh convergence check

Since the FEA mesh is very fine, no convergence testing based on mesh refinement was carried out. However, certain accuracy checks have been undertaken. For example, for the elastic model the maximum discontinuity in peak nodal stress predictions, from adjacent elements at the hole boundary, is less than 0.5%.

4.2 Typical stress results due to overload followed by unload

It is useful to consider stress distribution results due to overload and then followed by unloading for a specific case. The variation of plastic zone size with overload level is then also given.

4.2.1 Typical stress result due to overload followed by unload

The distributions of the stress quantities σ_{VM}, σ_{YY}, and σ_{XX} resulting from a compressive load of 654 MPa (equal to $0.5\sigma_Y$) are shown in Figure 7, along the prospective crack path $x = X / R$. For this overload, the plastic zone size is $D_{PZ} = 0.3R$, as indicated by the plastic zone size in Figure 7, where:

σ_{VM} is the von Mises stress;
σ_{YY} is the transverse, *y*-direction stress, along the prospective crack path;
σ_{XX} is the radial, *x*-direction stress, along the prospective crack path.

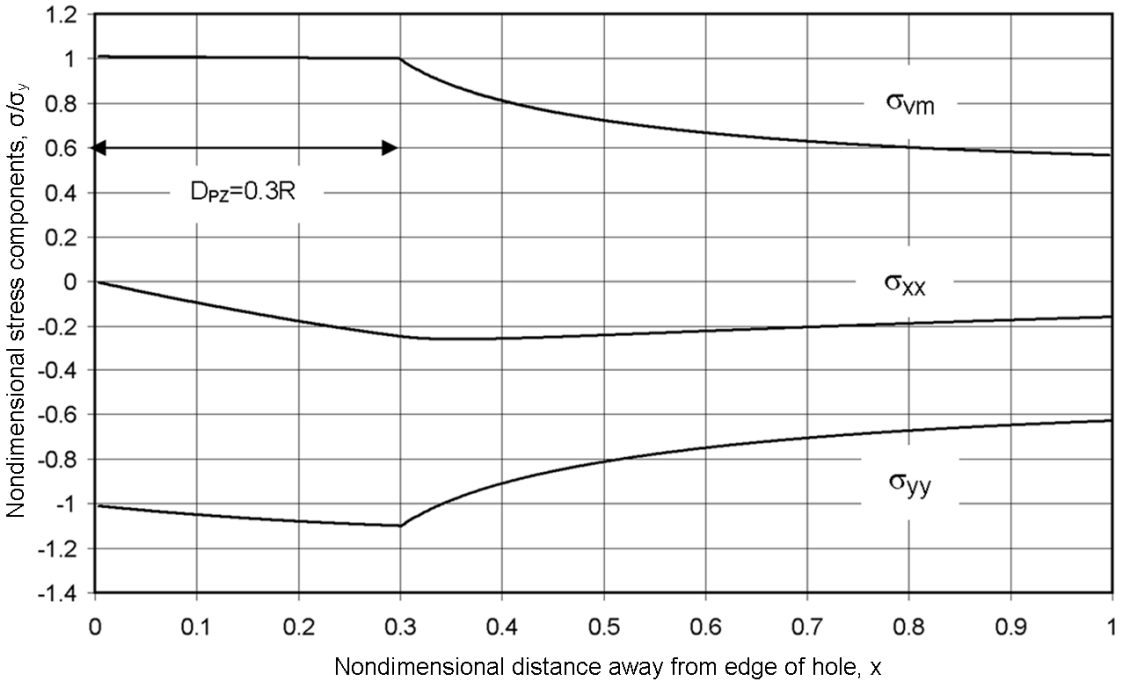

Figure 7: Normalised stress components along prospective crack path for plate with remote compressive overload

After the overload is removed, the resultant residual stresses along the prospective crack path where $y = 0$ are as shown in Figure 8. There is an inflection point in σ_{YY} and σ_{VM} at $x = 0.3$. Also, in this case σ_{YY} is a maximum at $x = 0$, and is of a value equal to $0.54\sigma_Y$ and for large x it asymptotes to zero. In comparison to σ_{YY}, the σ_{XX} stresses are low and hence the magnitude of σ_{VM} is almost the same as σ_{YY}.

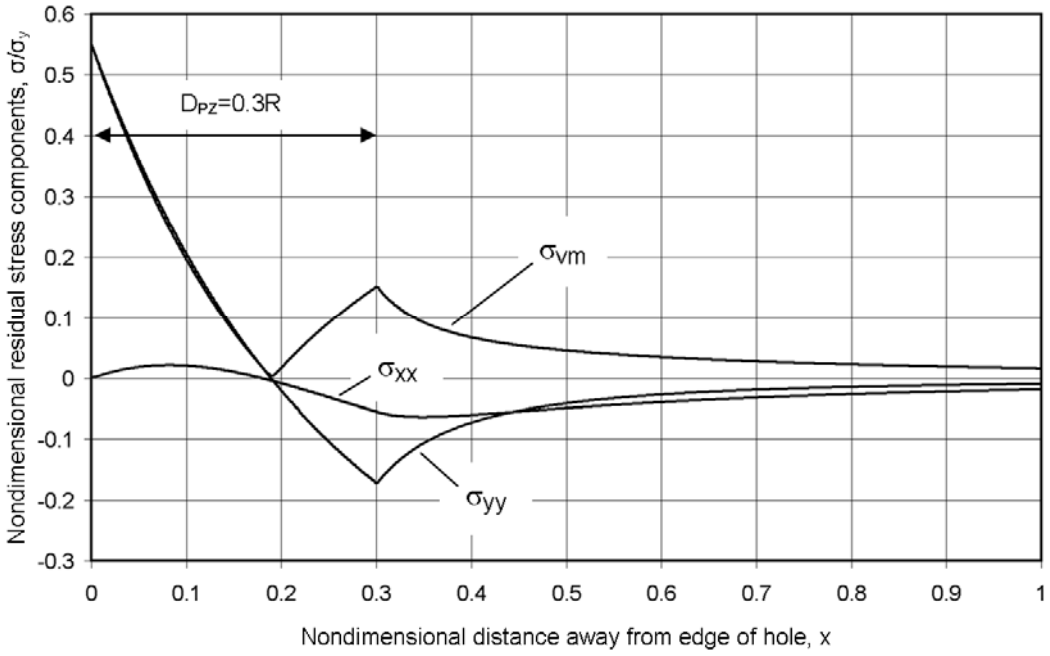

Figure 8: Residual stress components along prospective crack path for compressive overload followed by unload

Consider now a tensile overload of 654 MPa followed by an unload. The normalised residual stress σ_{YY}/σ_Y is shown in Figure 9. As expected, the sign of the value is the opposite to that given in Figure 8, but the magnitude is the same.

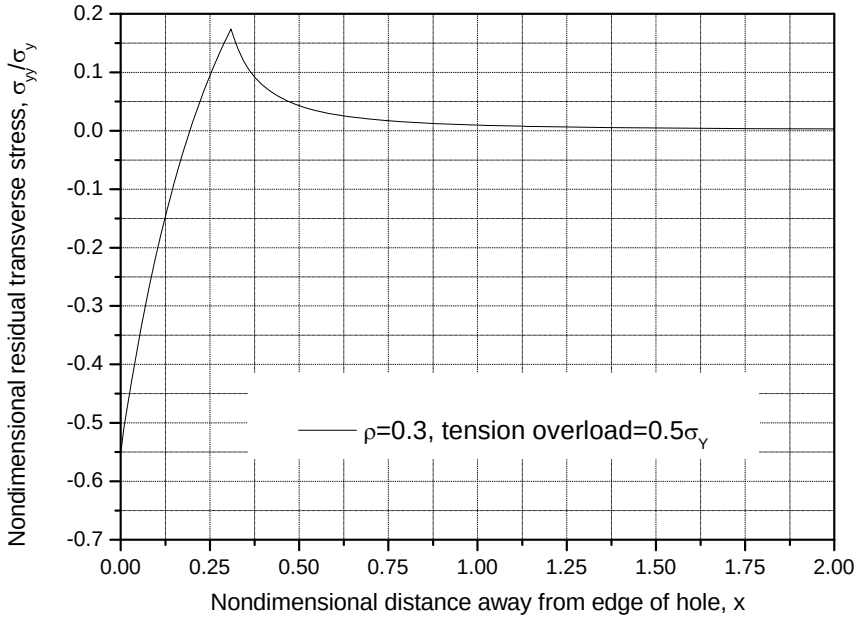

Figure 9: Residual transverse stress along prospective crack path for large D6ac steel plate for tensile overload followed by unload

4.2.2 Variation of plastic zone size with remote overload stress

Figure 10 gives the variation of the nondimensional plastic zone size $\rho = D_{PZ} / R$ with the magnitude of the compressive overload. This is a useful tool for determining the required initial overload stress σ_{ini} for any particular value of ρ required. This plot was used to obtain values of σ_{ini} for ρ = 0.1, 0.2 and 0.3, as needed in later sections.

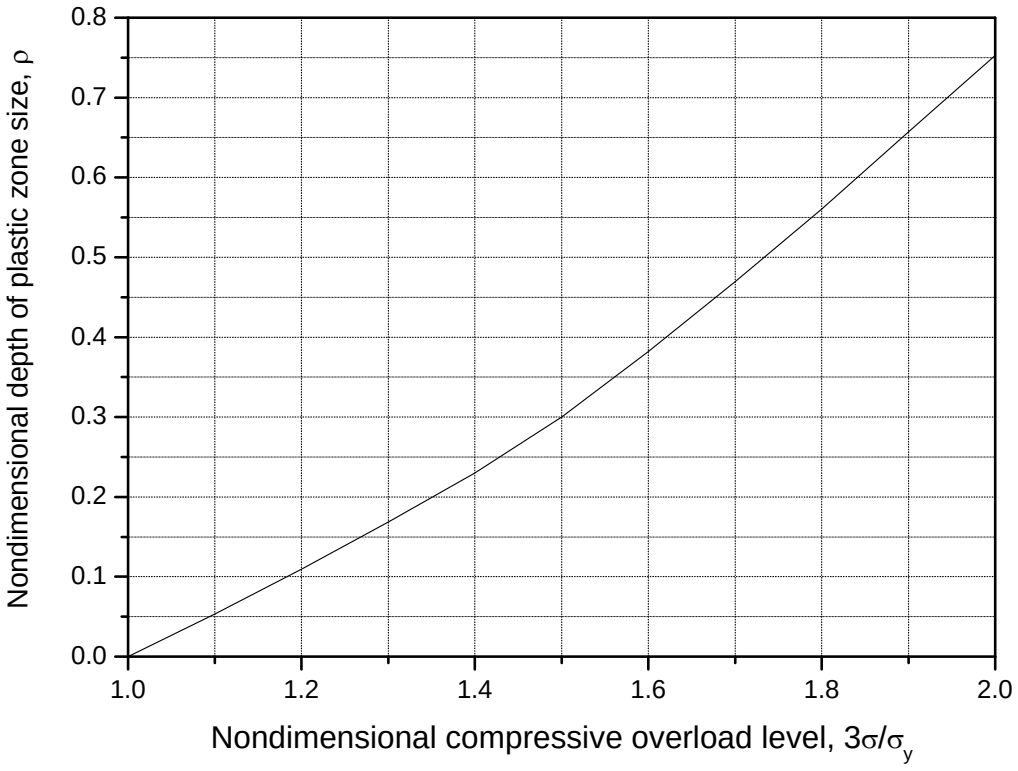

Figure 10: Depth of plastic zone versus level of compressive overload for a round hole in a unidirectional stress field

4.3 Comparison of typical stress results including service load

Shown in Figure 11 is the nondimensional transverse stress σ_{YY} / σ_Y for the case of a 654 MPa tension overload followed by an unload and then application of a 200 MPa service load. Also shown are the results for the 654 MPa compressive overload case. As expected, the tension overload results in a lowering of the residual stresses σ_{YY} / σ_Y near the hole, whereas the compression overload results in higher residual stresses. Note also that the edge of the initial yield zone is located at x = 0.3. As expected, for large x the two solutions converge.

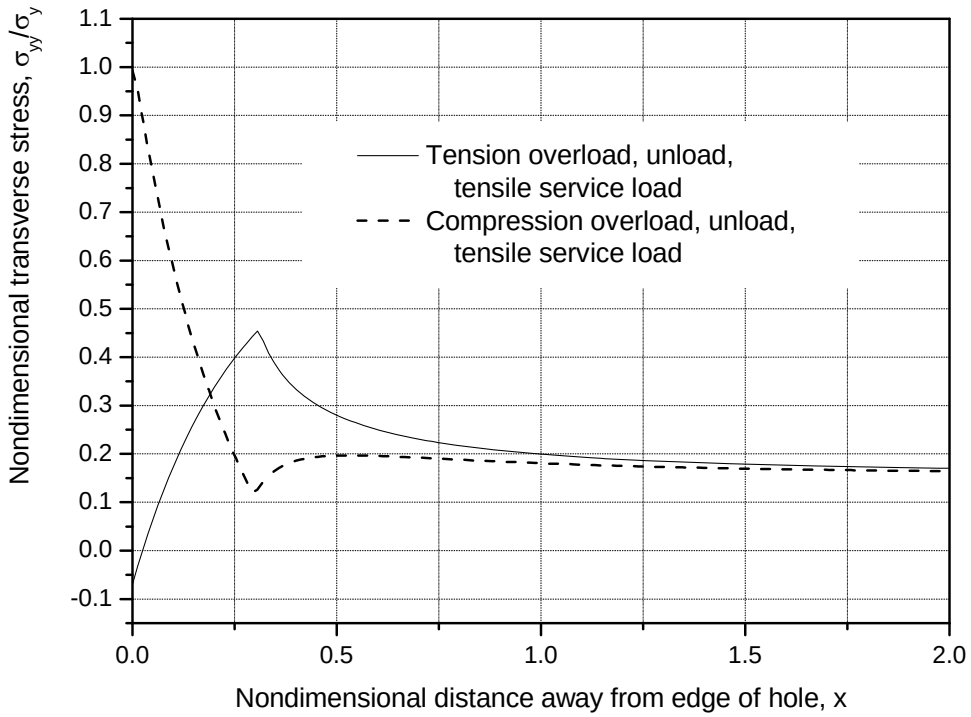

Figure 11: Transverse stress for overload with application of 200 MPa remote load

5. Weight function method for cracked hole in loaded plate

This section initially gives the definition of the weight function approach and an effective numerical integration technique for its calculation. Then stresses and stress intensity factors for the cold-expanded-hole case are given. A function for stress at the edge of a hole due to remote loading is also given to be used in determining the effect of subsequent remote service load.

5.1 Weight function definition

Consider an initial uncracked hole of radius R in a loaded plate as shown in Figure 12. The Mode I stress intensity factor, K_I, can be calculated from the integral of the product of the weight function, $m(x,a)$, and the transverse distribution of stress perpendicular to the prospective crack plane, $\sigma_{yy}(x)$. This is given by Bueckner [1] as:

$$K_I = \sqrt{W} \int_0^a \sigma_{yy}(x) m(x,a) dx \tag{2}$$

where W is a characteristic dimension, and for cracks emanating from a hole $W = R$.

For the case of a symmetric crack emanating from a hole in a large plate, it has been shown by Wu and Carlsson [3] that this weight function is given by:

$$m(x,a)=\frac{1}{\sqrt{2\pi a}}\sum_{i=1}^{3}\beta_i(a)\left(1-\frac{x}{a}\right)^{i-3/2} \tag{3}$$

where a nondimensional form of K_I is given by:

$$f=\frac{K_I}{\sqrt{\pi aR}} \tag{4}$$

where:

A is the crack length;
a is the crack length ratio, A/R;
x is the normalised distance from the hole edge, X/R;
$\sigma_{yy}(x)$ is the stress in the uncracked body transverse to the crack path at a distance x from the hole edge;
$\beta_i(a)$ are 3 handbook coefficient values (i = 1 to 3) taken from Wu and Carlsson [3], Table 13.1, with N = 2. Here $\beta_1(a)$ = 2.0, and $\beta_2(a)$ and $\beta_3(a)$ are functions of a, accurately represented by ninth-order polynomials.

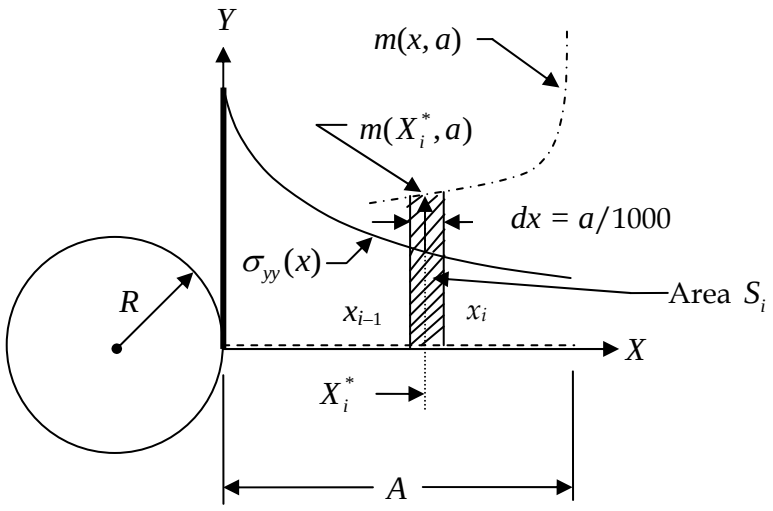

Figure 12: Notation and geometry for analysis of overloaded plate containing a hole and local detail for calculation of stress intensity factor

In this report the method of superposition will be used in conjunction with the weight function method for determining K_I due to combined residual stresses and stresses from

subsequent service loading. However, in some cases, negative K_I will be determined. The method of superposition is however only valid when the crack is open. The limits of validity (of crack sizes considered) will be established on a case-by-case basis. Here, the combined stresses along the crack path determine if the crack is fully open or if the crack is partially closed. For this formulation of the weight function method it is known that partial closure of the crack will introduce some error in the calculation of K_I depending also on the crack size.

5.2 Numerical integration method

In order to calculate the stress intensity factor as a function of crack length, the numerical method by Moftakhar and Glinka [27] is used. Reference [27] has proposed that the integral from Equation (2) can be calculated from Equation (5) below:

$$K_I = \sqrt{W} \sum_{i=1}^{n} S_i \sigma_{yy}(X) \tag{5}$$

This represents the product of the area, S_i , under the curve $m(x,a)$ and the value of the function $\sigma_{yy}(X)$. And this corresponds to the coordinate *X* of the centroid of the area S_i as shown in Figure 12. In [27] this procedure is reversed as:

$$K_I = \sqrt{W} \sum_{i=1}^{n} S_i^* m(X_i^*, a) \tag{6}$$

This procedure is implemented by calculating the areas S_i^* under the stress function $\sigma_{yy}(x)$ and the coordinates X_i^* of their centroids. This leads to:

$$S_i^* = \frac{1}{2}\left[\sigma_{yy}(x_i) + \sigma_{yy}(x_{i-1})\right](x_i - x_{i-1}) \tag{7}$$

where x_i is the *x* coordinate of increment *i*, and x_{i-1} the *x* coordinate of the previous increment and X_i^* is given by:

$$X_i^* = x_i - \frac{(x_i - x_{i-1})\left[2\sigma_{yy}(x_{i-1}) + \sigma_{yy}(x_i)\right]}{3\left[\sigma_{yy}(x_i) + \sigma_{yy}(x_{i-1})\right]} \tag{8}$$

The weight function $m(X_i^*, a)$ is given by Equation (3), and the numerical procedure to solve for K_I has been implemented in a Fortran program (see Appendix A). Also the procedure adopted here uses strips of width $dx = a/1000$ and the integration is taken up to a. Since $m(x,a)$ is never evaluated any closer than $dx/2$ from $x = a$ the singularity in $m(x,a)$ at $x = a$ in Equation (3) is avoided.

It should be noted that, in order to represent the transverse stresses in the computer program, a 4th-order polynomial was used in the initial yield zone and an exponential decay was used outside this region (see Figure 11).

5.3 Comparison for remote loading case

It is useful to confirm the accuracy of the numerically determined value of K_I, by comparison with a known analytical solution, for the remote-loading case that is shown in Figure 3. For the numerical solution the equation for the stress, σ_{YYre}, away from the edge of a hole in an infinite plate for elastic conditions, is used. This is given by Timoshenko and Goodier [28]:

$$\sigma_{YYre} = \sigma_{re}\left[1+\frac{0.5}{(1+x)^2}+\frac{1.5}{(1+x)^4}\right] \tag{9}$$

where x is the nondimensional distance ahead of the hole and σ_{re} is the remote stress. Hence, the normalised stress intensity factor, f, is determined numerically using Equations (2), (3), (4) and (9), and the results are given in Figure 13. The corresponding analytical solution by Wu and Carlsson [3] is also given, showing very good agreement.

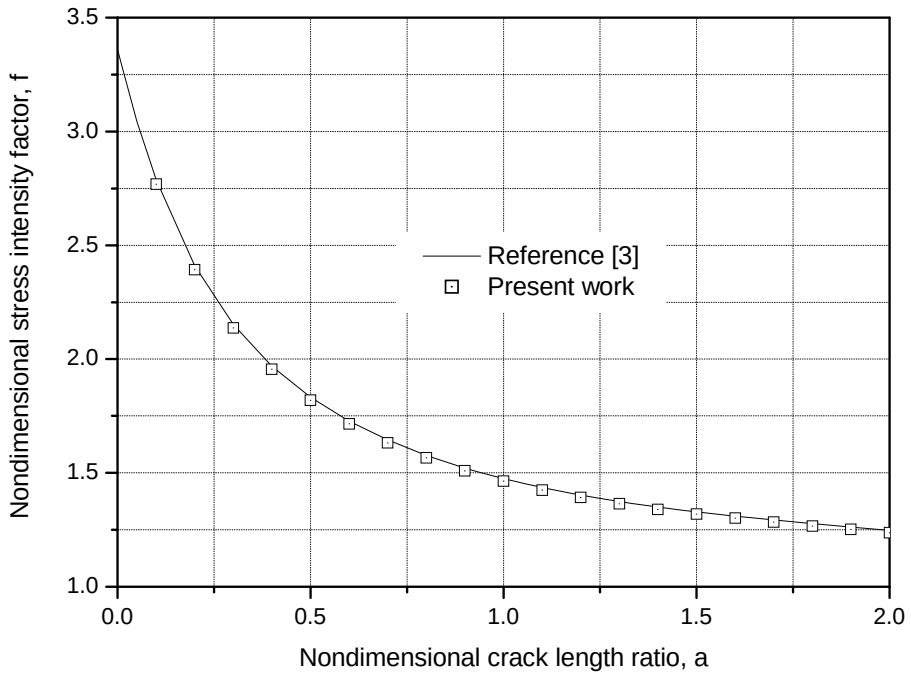

Figure 13: Comparison of function f for a cracked hole in loaded plate versus crack length ratio

5.4 Stresses and stress intensity factor for cold-expanded hole (no remote load)

A state of plane strain is assumed in all analyses involving the cold-expanded hole unless noted otherwise in order to compare with existing analytical solutions. It is also important to note that an elastic–perfectly plastic yield condition is assumed in the stress response analysis[1]. In order to determine the nondimensional initial plastic yield zone size, $\rho = D_{PZ} / R$, corresponding to the interference level λ, the following equation is used (see Equation (64) of Jost [29]):

$$\lambda = \frac{\sigma_y}{E\sqrt{3}}\left[(1+\nu)(1+\rho)^2\left(1+(1-2\nu)\left(\frac{\rho R+R}{w}\right)^2\right)\right.$$

$$\left.+(1+\nu_M)(1-2\nu_M)\frac{E}{E_M}\left(\ln(1+\rho)+1-\left(\frac{\rho R+R}{w}\right)^2\right)\right] \qquad (10)$$

where ν_M and ν are the Poisson's ratio for the mandrel and plate respectively, and E_M is the modulus of elasticity for the mandrel.

5.4.1 Removal of mandrel resulting in residual stresses for case of no re-yielding

The geometry and idealised yielding case considered here is shown in Figure 14. It is assumed there is no re-yielding at the hole edge when the mandrel is removed.

[1] Hence, some small discrepancy is expected in the stress prediction as compared to any analysis using the strain hardening assumption based on the material properties in Table 1.

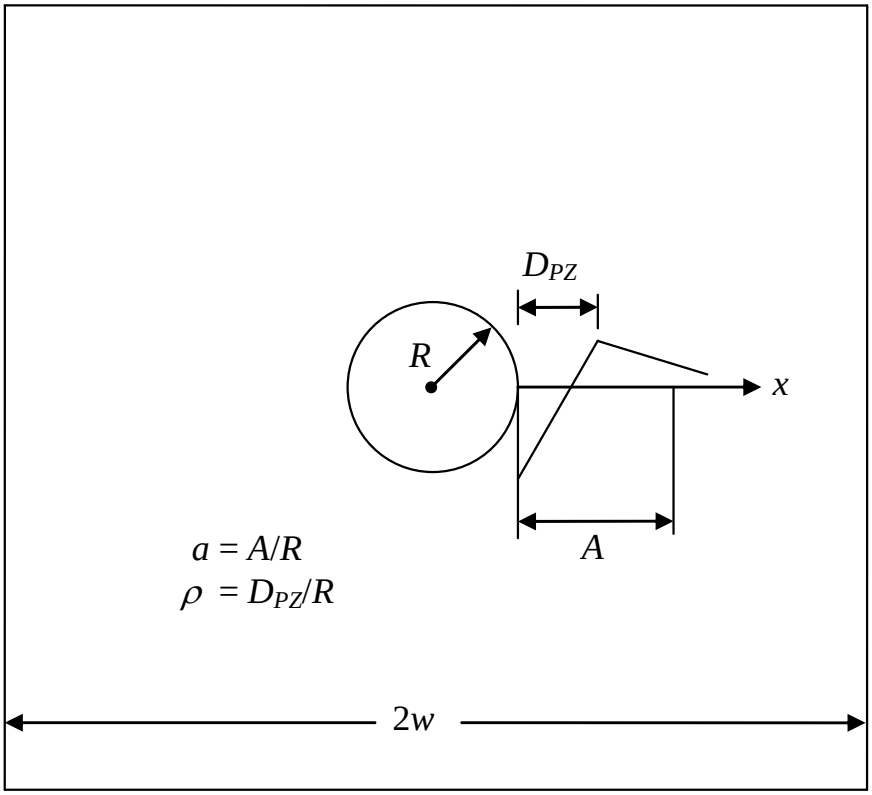

Figure 14: Geometry and idealised yielding cases for a cold-worked hole in a remotely-loaded finite-width plate with no re-yielding following removal of mandrel

Rich and Impellizzeri [30] have derived the residual stress distributions around a hole in which a mandrel has been inserted to cause plastic deformation, and then removed. This induces a self-equilibrating residual stress field. For convenience, the derivation used here is given by Jost [29]. The residual tangential stress, σ_T along the prospective crack path $y = 0$, for an elastic–perfectly plastic material and plane strain condition for $x \le \rho$ is given by:

$$\sigma_{yy}(x) = \sigma_T = \frac{\sigma_y}{\sqrt{3}}\left\{2\ln\left(\frac{1+x}{1+\rho}\right)+1+\left(\frac{R+\rho R}{w}\right)-\alpha\left[\left(\frac{1}{1+x}\right)^2-\left(\frac{R}{w}\right)^2\right]/\left[1-\left(\frac{R}{w}\right)^2\right]\right\} \quad (11)$$

For $\rho \le x \le w$:

$$\sigma_{yy}(x) = \sigma_T = \frac{\sigma_y}{\sqrt{3}}\left\{\left(\frac{1+\rho}{1+x}\right)^2+\left(\frac{R+\rho R}{w}\right)^2-\alpha\left[\left(\frac{1}{1+x}\right)^2-\left(\frac{R}{w}\right)^2\right]/\left[1-\left(\frac{R}{w}\right)^2\right]\right\} \quad (12)$$

From Jost [29] and converting to the present notation, the residual radial stress for $x \le \rho$ is given by:

$$\sigma_{xx}(x)=\sigma_R=\frac{\sigma_y}{\sqrt{3}}\left\{2\ln\left(\frac{1+x}{1+\rho}\right)-1+\left(\frac{R+\rho R}{w}\right)^2+\alpha\left[\left(\frac{1}{1+x}\right)^2-\left(\frac{R}{w}\right)^2\right]/\left[1-\left(\frac{R}{w}\right)^2\right]\right\} \quad (13)$$

while for $x \geq \rho$ the radial stress is given by:

$$\sigma_{xx}(x)=\sigma_R=\frac{\sigma_y}{\sqrt{3}}\left\{-\left(\frac{1+\rho}{1+x}\right)^2+\left(\frac{R+\rho R}{w}\right)^2+\alpha\left[\left(\frac{1}{1+x}\right)^2-\left(\frac{R}{w}\right)^2\right]/\left[1-\left(\frac{R}{w}\right)^2\right]\right\} \quad (14)$$

where α is given by:

$$\alpha=2\ln(1+\rho)+1-\left(\frac{R(1+\rho)}{w}\right)^2 \quad (15)$$

Another Fortran program has been written to compute *f*, the nondimensional stress intensity factor, using weight functions from Equations (3) and (6)–(8) and Equations (4) and (11)–(12). As a check on the computer code accuracy, results for *f* obtained using the present method, as *R*/*w* approaches zero, are shown in Figure 15, together with the corresponding results from Wu and Carlsson [3]. Here, good agreement is seen.

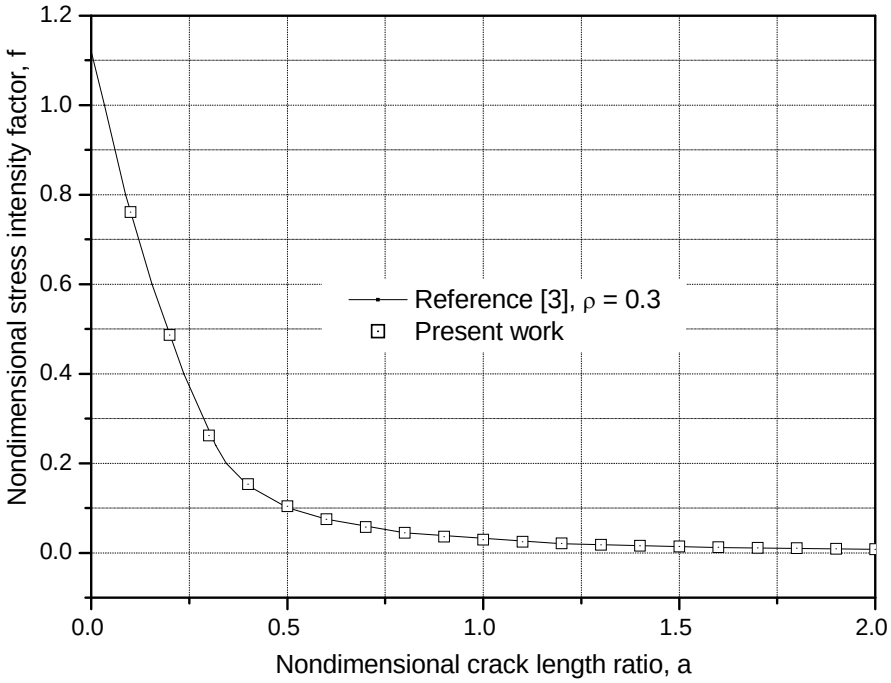

Figure 15: Comparison of f for a cold-worked hole versus crack length ratio

5.4.2 Removal of mandrel resulting in re-yielding

Here, we consider the case where during removal of the mandrel re-yielding occurs adjacent to the hole, as idealised in Figure 16. A peak transverse stress exists at $x = R_{RY} - R$.

It can be shown from Jost [29] that the re-yield radius for an infinite plate is given by:

$$R_{RY} = \sqrt{R^2(1+\rho)}\; e^{-0.25} \tag{16}$$

The re-yield radius for a finite-width plate is given by:

$$R_{RY} = \sqrt{R^2(1+\rho)}\; e^{-0.25\left(1+\left(\left(\frac{R(1+\rho)}{R_{RY}}\right)^2-2\right)\left(\frac{R_{RY}}{w}\right)^2\right)} \tag{17}$$

This allows for an iterative solution for R_{RY}. The nondimensional re-yield radius, η, is given by:

$$\eta = (R_{RY} - R)/R \tag{18}$$

The following expressions for the tangential stress are all derived from Jost [29] and apply along the prospective crack path where $y = 0$:

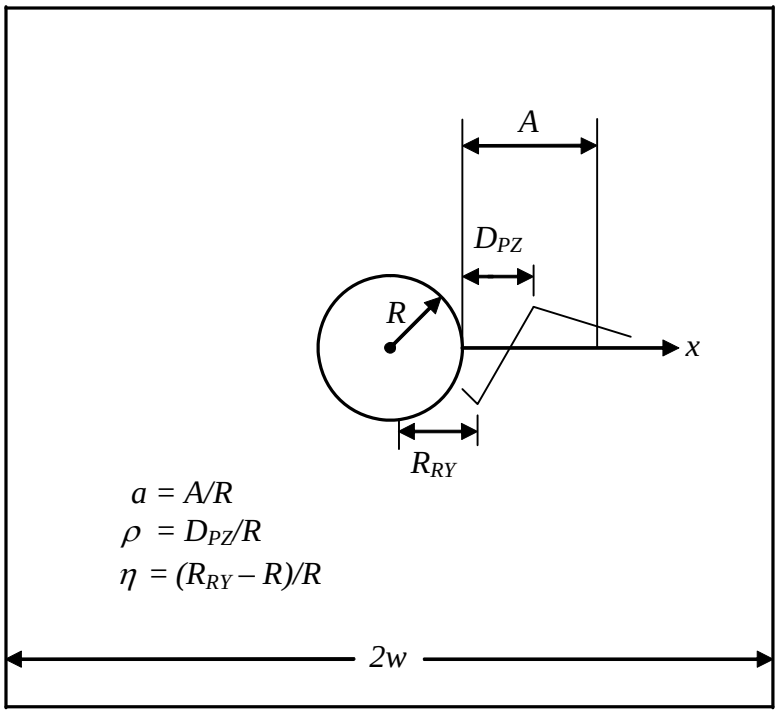

Figure 16: Geometry and idealised yielding cases for a cold-worked hole in a remotely-loaded finite-width plate with re-yielding following removal of mandrel

For $0 \le x \le \eta$ we have:

$$\sigma_{yy}(x) = \sigma_T = -\frac{2\sigma_y}{\sqrt{3}}\left(1+\ln(1+x)\right) \tag{19}$$

For $\eta \le x \le \rho$ we have:

$$\sigma_{yy}(x) = \sigma_T = \frac{\sigma_y}{\sqrt{3}}\left\{2\ln\left(\frac{1+x}{1+\rho}\right)+1+\left(\frac{R(1+\rho)}{w}\right)^2-2\left\{\left(\frac{\eta}{1+x}\right)^2+\left(\frac{R\eta}{w}\right)^2\right\}\right\} \tag{20}$$

And for $\rho \le x \le w$ we have:

$$\sigma_{yy}(x) = \sigma_T = \frac{\sigma_y}{\sqrt{3}}\left\{\left(\frac{1+\rho}{1+x}\right)^2+\left(\frac{R(1+\rho)}{w}\right)^2-2\left\{\left(\frac{\eta}{1+x}\right)^2+\left(\frac{R\eta}{w}\right)^2\right\}\right\} \tag{21}$$

These equations are sufficient to generate the entire stress solution for $0 \le x \le w - R$.

5.4.3 Reaming after re-yielding

Although they are not used in the present work, for completeness the stress equations corresponding to reaming after re-yielding are also given here. Usually after cold working, the hole will be reamed out, increasing the size of the hole (to create a smooth undamaged surface). The following equations from Jost [29] are used. As before, ρ is determined from Equations (1) and (10). Firstly, due to the cold expansion we have the real radius of the hole:

$$R_{REAL} = (1+\lambda)R \tag{22}$$

Due to the reaming radius, R_{REAM}, we have the increment for the change of hole radius:

$$\delta a = R_{REAM} - R_{REAL} \tag{23}$$

From Equation (35) of Jost [29] we have the following equation to determine the new re-yield radius, R^*_{RY}:

$$\ln\left((R+\delta a)/R\right) = 2\ln(R^*_{RY}) + (R_{RY}/w)^2 - (R^*_{RY}/w)^2 \tag{24}$$

The nondimensional re-yield radius is given by:

$$\eta = \left(R^*_{RY} - (R+\delta a)\right)/\left(R+\delta a\right) \tag{25}$$

The following stresses apply along the prospective crack path where $y = 0$:

For $\eta \le x \le \rho$ we have:

$$\sigma_{yy}(x) = \sigma_T = -\frac{2\sigma_y}{\sqrt{3}}\left(1+\ln(1+x)\right) \tag{26}$$

For $\eta \le x \le \rho$ we have:

$$\sigma_{yy}(x) = \sigma_T = \frac{\sigma_y}{\sqrt{3}}\left\{2\ln\left(\frac{1+x}{1+\rho}\right)+1+\left(\frac{(R+\delta a)(1+\rho)}{w}\right)^2-2\left\{\left(\frac{\eta}{1+x}\right)^2+\left(\frac{(R+\delta a)\eta}{w}\right)^2\right\}\right\} \tag{27}$$

And for $\rho \le x \le w$ we have:

$$\sigma_{yy}(x) = \sigma_T = \frac{\sigma_y}{\sqrt{3}}\left\{\left(\frac{1+\rho}{1+x}\right)^2+\left(\frac{(R+\delta a)(1+\rho)}{w}\right)^2-2\left\{\left(\frac{\eta}{1+x}\right)^2+\left(\frac{(R+\delta a)\eta}{w}\right)^2\right\}\right\} \tag{28}$$

These equations are sufficient to generate the entire stress solution for $0 \le x \le w-R$. It has been found that in practice very little difference exists between the unreamed re-yielded solution and the reamed re-yielded solution.

5.5 Elastic stress for finite-width plate

The equations above for the tangential stress contain a finite-width dimension w, as defined in Figure 1. However, to combine with an elastic remote stress also requires a finite-width capability. The following equation, for the elastic stress in the neighbourhood of a circular hole in a finite-width plate, taken from Howland [31], is used:

$$\sigma_{YYre}(x) = \sigma_{re}\left\{1+2m_o+\frac{d_0}{(R(1+x)/w)^2}+2\sum_{n=1}^{\infty}\frac{n(2n+1)d_{2n}}{(R(1+x)/w)^{2n+2}}+\frac{(n-1)(2n-1)e_{2n}}{(R(1+x)/w)^{2n}}\right.$$

$$\left.+n(2n-1)l_{2n}(R(1+x)/w)^{2n-2}+(n+1)(2n+1)m_{2n}(R(1+x)/w)^{2n}\right\} \tag{29}$$

where m_n, d_n, e_n, l_n are coefficients defined in Howland [31], σ_{re} is the remote stress, and the normalised distance from the hole edge is given by $x = X/R$. The only limitation is: $\left|\sigma_{YYre}+\sigma_{YYrs}\right| \le \sigma_y$, where σ_{YYre} is obtained from Equation (29) above and σ_{YYrs} is the residual stress defined in section 5.4.1 or 5.4.2 or 5.4.3. As a check, $\sigma_{YYre}/\sigma_{re}$ is plotted against $R(1+x)/w$ for different R/w ratios, as shown in Figure 17. Data points taken from [29] are also shown in Figure 17, and these show good agreement with the curves. This validates this section of the computer code developed to implement the analysis.

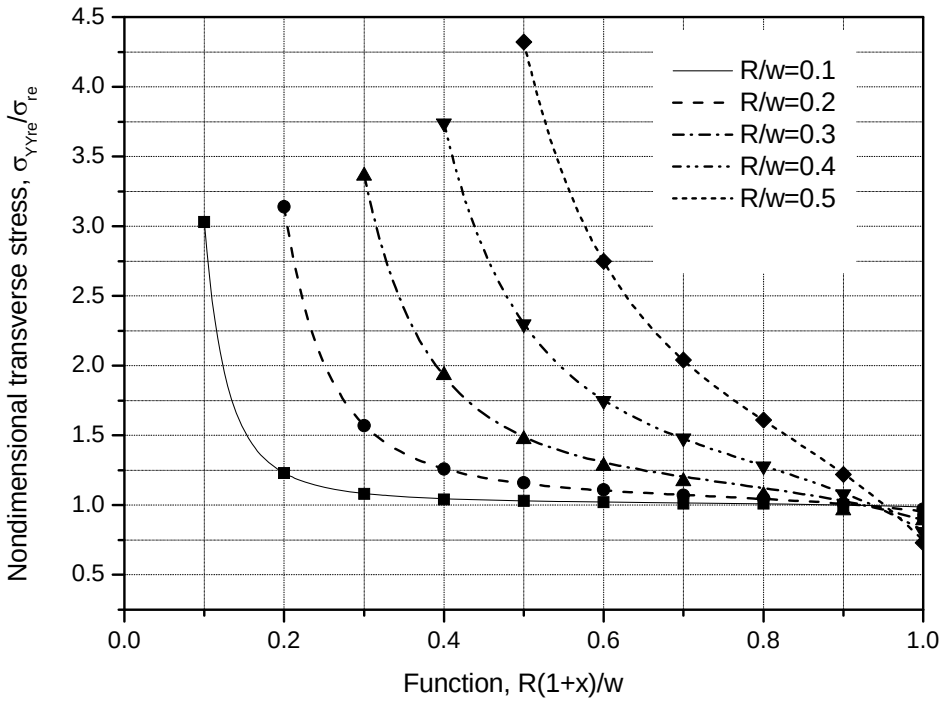

Figure 17: Transverse stress $\sigma_{YYre} / \sigma_{re}$ versus $R(1+x)/w$ for different R/w, using analysis given in [31]

6. Cold-expanded hole subject to remote loading – weight function method

In this section, three cases for cold-expanded holes are considered as follows: (i) hole in a generic large D6ac steel plate; (ii) hole in a generic large aluminium alloy plate including comparison with published results; and (iii) application to a hole in C-130 wing skin location, with a finite-width geometry, with associated checks on closure effects. All cases assume conditions of plane strain.

6.1 Application to a hole in a large D6ac steel plate

For a range of initial plastic yield zone sizes using Equations (6)–(8), the tangential stress variation away from a cold-worked hole has been determined and is shown in Figure 18. For completeness, the radial stresses are also given in Figure 19 for various nondimensional plastic zone sizes, ρ. In order to determine the range of validity of the solution for the stress intensity factor, the sum of the residual stresses and those due to subsequent remote loading stress are given in Figure 20, along the prospective crack path. The remote stress is 200 MPa, and it is seen that for these results, for $\rho = 0.1$ and 0.2, that the crack is fully open (i.e.

$\sigma_{yy} / \sigma_y > 0$). However, for $\rho = 0.3$ there is crack closure between $0 \leq a \leq 0.084$, and K_I, as calculated on the basis of a fully-open crack, is not valid. With $a > 0.084$, the crack is partially open and there is some error in K_I, which reduces for increasing a.

Using the tangential residual stress results, a Fortran program has been written using weight functions to compute the residual stress intensity factor caused by cold working of the hole by a mandrel. These results are shown in Figure 21 and indicate a maximum value of –763 MPa mm$^{0.5}$ at a distance of 0.6 mm for $\rho = 0.3$. For smaller initial plastic zone sizes, the maximum value of K_I is reduced and the peak value occurs at a smaller crack length ratio. As shown in Equations (10)–(12), the smaller the initial plastic zone size the smaller the interference. Similar curves have been obtained by Moreira et al [20] for plane stress conditions also using a weight function approach, but for an aluminium alloy plate instead of D6ac steel.

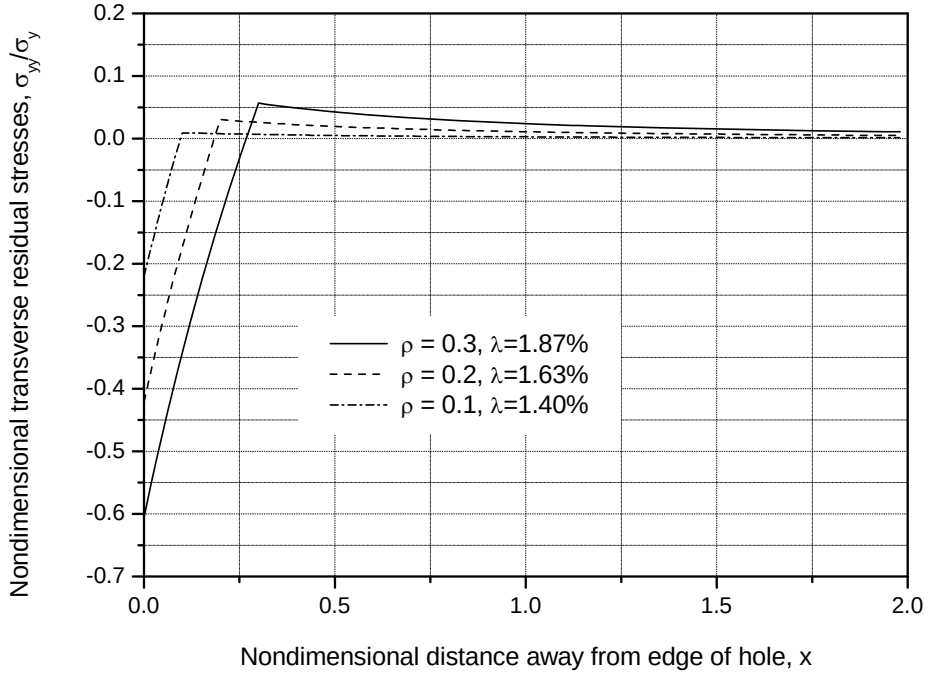

Figure 18: Transverse residual stresses along prospective crack path for a large D6ac steel plate due to cold working followed by removal of mandrel

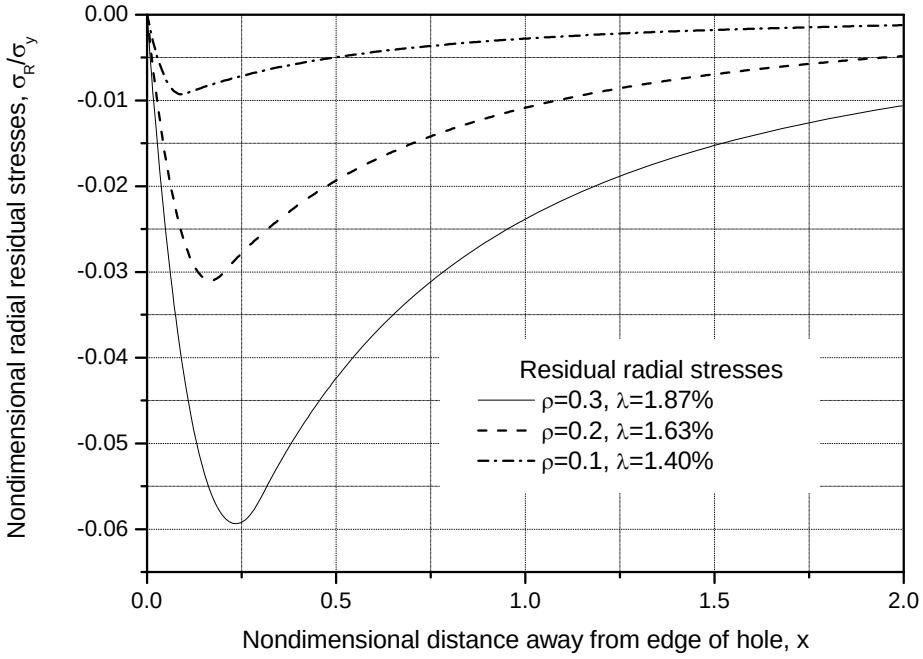

Figure 19: Radial residual stresses along prospective crack path for a large D6ac steel plate due to cold working followed by removal of mandrel

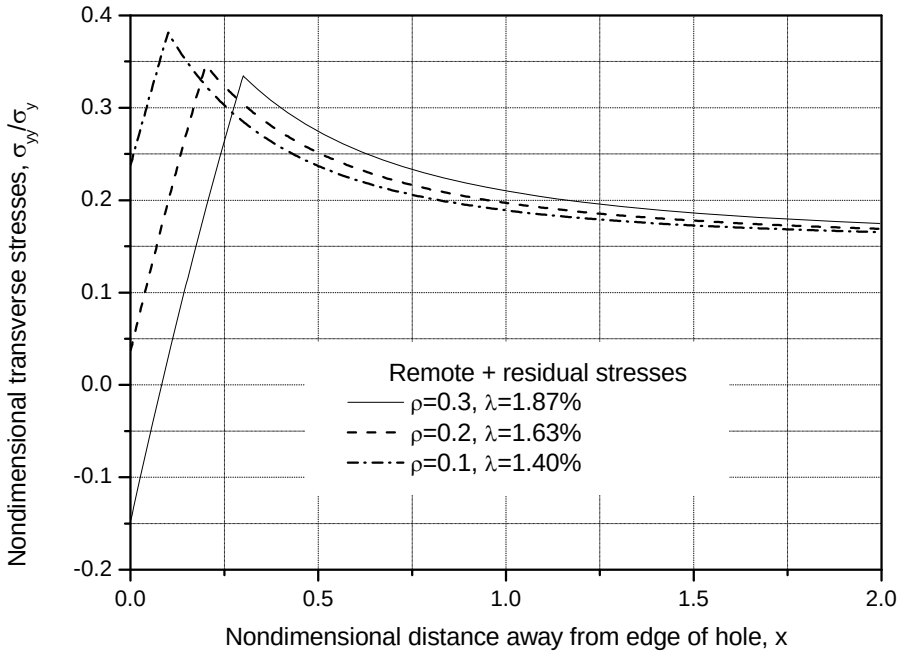

Figure 20: Transverse stresses along prospective crack path for a large D6ac steel plate due to cold working and effect of subsequent remote stress of 200 MPa

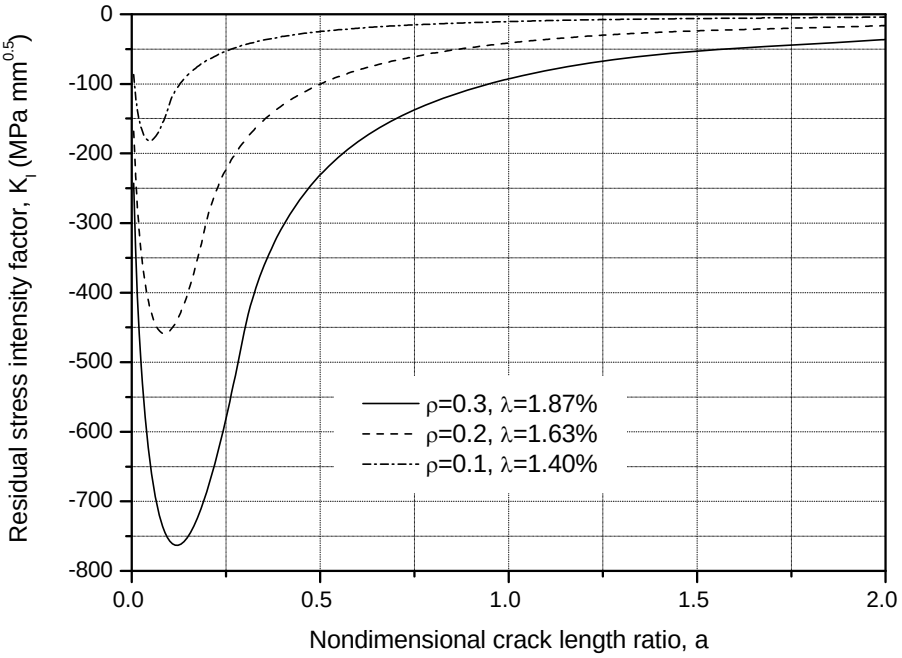

Figure 21: Stress intensity factor results for a cold-worked hole in a large D6ac steel plate from residual stress

To investigate the beneficial effects of cold working under realistic conditions, a combined loading, using the method of superposition, has been considered, with a remote tensile stress of 200 MPa and initial plastic yield zone sizes of ρ = 0.1, 0.2 and 0.3. As for previous cases, the geometry is for a 5 mm radius hole. These results are shown in Figure 22, together with the results for the case of remote stress alone. Clearly, the cold working is beneficial, both within the initial yield zone and extending some distance outside the initial yield zone, with the best results being obtained with the largest initial plastic yield zone.

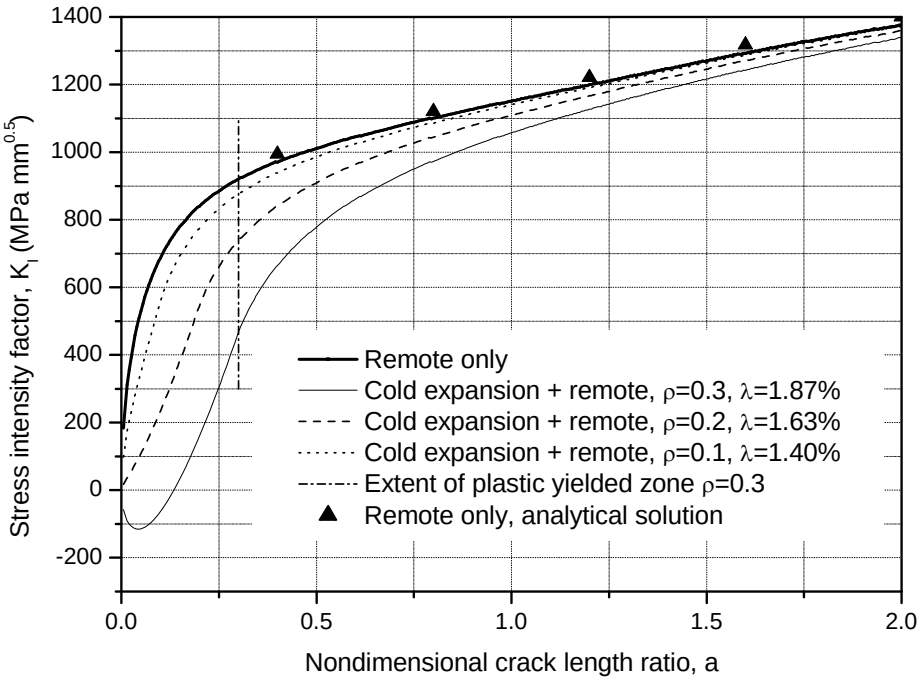

Figure 22: Stress intensity factor results for a cold-worked hole in a large D6ac steel plate with subsequent remote tensile stress of 200 MPa

6.2 Comparison with previous work for a large aluminium alloy plate

For the cold-worked hole, the most relevant published data that have been found are those of Moreira et al [20]. However, they correspond to an infinite aluminium plate under plane stress conditions. Since the present work uses conditions of plane strain, an approximate comparison was made by adjusting the interference in the present analysis in order to achieve the same residual stress as shown in Figure 23. Here, it was found that the use of λ = 1.15% for plane strain closely agrees with λ = 2.00% for the plane stress case analysed in Moreira et al [20]. The geometry used is presented in Table 2, and the equations used were Equations (19) and (21)–(23). The definition of interference used in Moreira et al [20] is the same as that in Equation (1). Also, from a private communication with the corresponding author, it was established that the von Mises yield criterion was used. Note that, in Figure 23, in the set of results shown for Moreira et al [20], the value for x = 0. This corresponds to $\sigma_{YY} = \sigma_Y$ = 285 MPa, which confirms that conditions of plane stress are being used. Also, while re-yielding occurs in Moreira et al [20], which also occurs in our analysis, there is disagreement at x = 0, since in plane strain $\sigma_{YY} = 2\sigma_Y / \sqrt{3}$ = 329 MPa. The corresponding residual stress intensity factor for both the present work and that from Moreira et al [20] is shown in Figure 24 and involves a disagreement of 7.5%. The reason for the disagreement is not clear. However, in the weight function method used, the radial stresses will not contribute to the stress intensity factor, when using a J-integral method within FEA a contribution is possible. The typical

normalised tangential and radial stresses for a cold-worked hole in an aluminium alloy plate are shown in Figure 25. This corresponds to 1% interference. From this it can be seen that compressive radial stresses exist along the prospective crack path.

Table 2: Parameters for calculation of interference and assumptions made

Quantity	Present work	Moreira et al [20]
E_M	207000 MPa	Not applicable[1]
E_P	71400 MPa	71400 MPa
σ_y	285 MPa	285 MPa
R	10 mm	10 mm
b	finite plate, w/R=10	finite plate, w/R=10
ν_M	0.3	Not applicable[1]
ν_P	0.3	0.3
ρ	0.875	0.875
λ	0.0115 (1.15%)	0.02 (2%)
Plane strain	Yes	No
Plane stress	No	Yes
Perfectly elastic–plastic	Yes	Yes
Re-yield at hole	Yes	Yes
Yield criteria	von Mises	von Mises[2]

[1] Interference was applied as an imposed displacement.

[2] From private communication with corresponding author (the yield criterion that was used was not specified in journal paper).

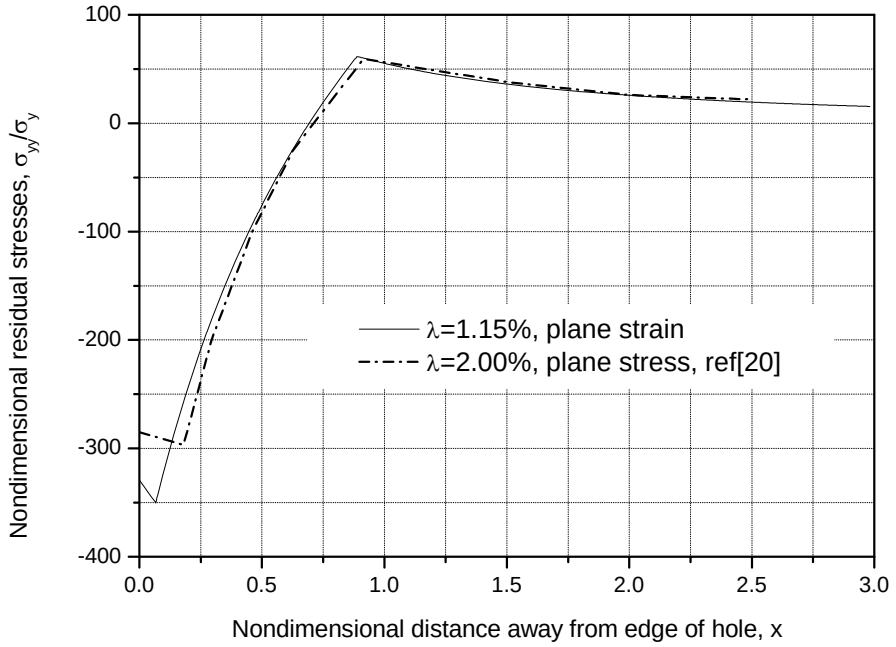

Figure 23: Residual stresses along prospective crack path due to cold expansion in a large aluminium plate, comparison with work in [20]

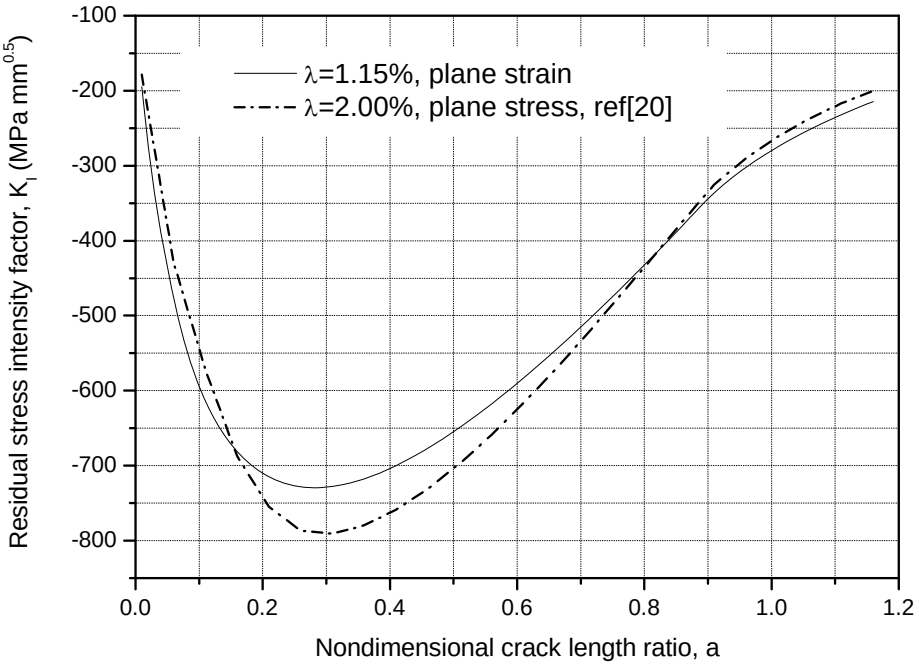

Figure 24: Stress intensity factor due to residual stress in a cold-worked large aluminium plate for 1.15% interference; comparison with work in [20]

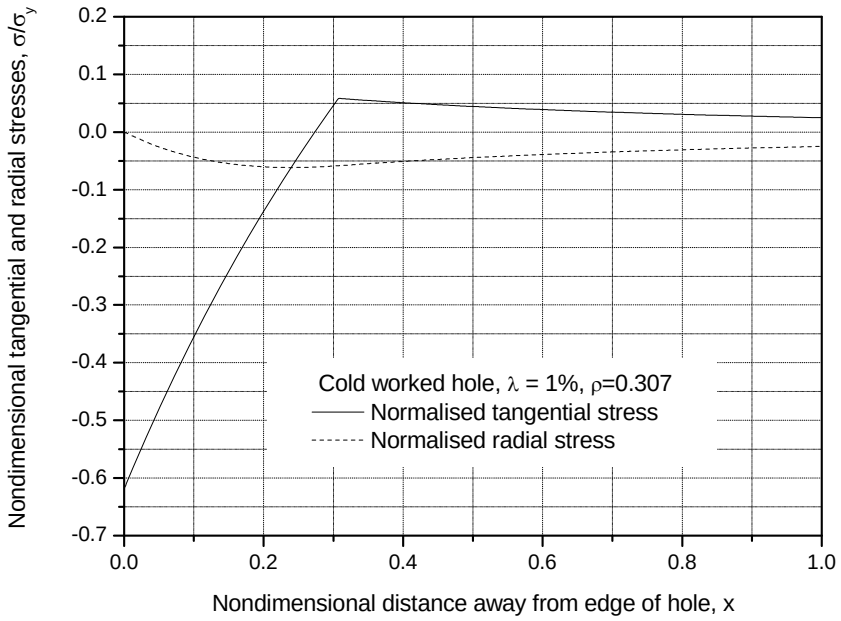

Figure 25: Plot of nondimensional tangential and radial stresses away from a cold-worked hole in an aluminium plate

6.3 Application of cold-expanded hole to C-130 wing

DSTO is embarking on a substantive coupon test program in support of likely life extension modifications of the C-130 transport aircraft at fatigue hotspots. A typical location where cold expansion is being considered is at the lower wing skin holes, as shown in Figure 26 and Figure 27. Therefore, to assist in the interpretation of the pending fatigue test results, here predicted K_I results are determined for the coupon geometry being tested. This coupon is made from an aluminium alloy whose properties are given in Table 3. A coupon of total width $2w$ = 32 mm and with a central hole of radius R = 3.0 mm is to be tested (w/R = 5.33), and it is assumed to be representative of this structure.

Table 3: Properties of C-130 lower wing skin at CW1

Material	Young's Modulus	Poisson's Ratio	Compression Yield Stress	Hole Radius
7075-T7351	71000 MPa	0.33	372 MPa	3.0 mm

Based on the cold-expansion equations in Section 5.4.2, shown in Figure 28 is a plot of nondimensional tangential stress, $\sigma_{yy}(x)/\sigma_y$, versus the nondimensional distance x away from the hole for three interference levels. The original yielded zone is also evident along with the re-yielded zone. The general trend is for higher peak values (both positive and negative) to occur for increasing levels of interference. Furthermore, the peak values occur at increasing distances away from the hole for increasing interference. For this finite-width plate, the

positive values of $\sigma_{yy}(x)/\sigma_y$ peak at x = 2.3 corresponding to 5% interference, where the peak positive nondimensional stress is σ_{yy}/σ_y = 0.53.

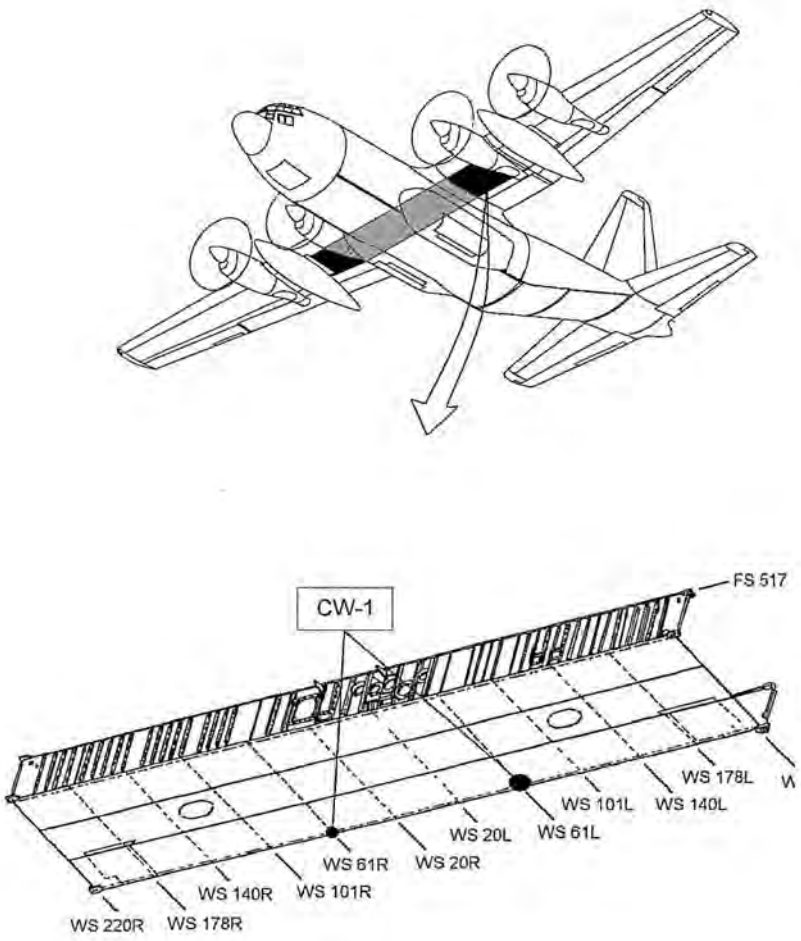

Figure 26: Location of cold-expanded hole on lower wing skin of C-130

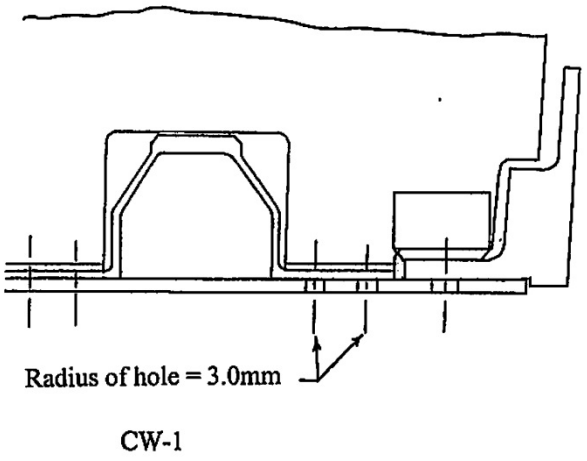

Figure 27: Local detail of C-130 hole subject to cold expansion, looking in spanwise direction

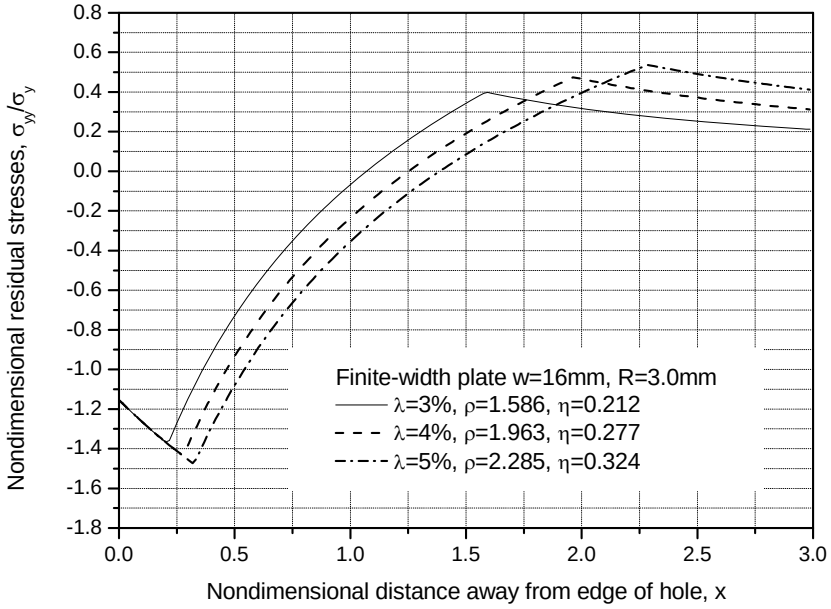

Figure 28: Residual stresses along prospective crack path due to cold expansion in a finite-width aluminium alloy plate representing C-130 fatigue test coupons (w/R = 5.33)

For comparison purposes, corresponding analyses for a large plate with w/R = 3333 have also been undertaken, in order to simulate the behaviour of an infinite plate. The tangential stress results are given in Figure 29. It can be seen that the positive values of nondimensional stress $\sigma_{yy}(x)/\sigma_y$ peak at x = 2.55 for 5% interference level, where the peak positive nondimensional stress is σ_{yy}/σ_y = 0.38. Hence, it is apparent that the peak positive stresses are significantly lower for the simulated infinite plate compared to those for the finite-width plate. On the

other hand, the magnitudes of the peak negative stresses for the finite-width plate were found to be marginally lower in comparison to those for the large plate. The extent of the zone of reversed yielding is also smaller for the finite-width plate than for the simulated infinite plate. Hence, it is important that the finite width be considered when interpreting fatigue test results.

Although the analysis presented here is based upon 2D plane strain conditions, it is useful to compare residual stresses with a full 3D FEA performed by Houghton and Campbell [32]. For an aluminium alloy plate with the same interference level of 3%, the same residual stress trends are predicted. As expected, at the mid-plane of the 3D analysis good agreement occurred with the (plane strain) 2D peak values, but the *x* coordinate of the 3D peak result was lower. At the surface of the 3D analysis, the peak values were lower; however, the *x* coordinates of the peaks were in agreement.

Using the weight function technique, the residual stress intensity factor obtained for the plate with $w/R = 5.33$ representing the C-130 test coupons has been plotted in Figure 30. The greatest negative stress intensity factor is achieved with the highest level of interference of 5%, while the lowest is achieved with an interference level of 3%.

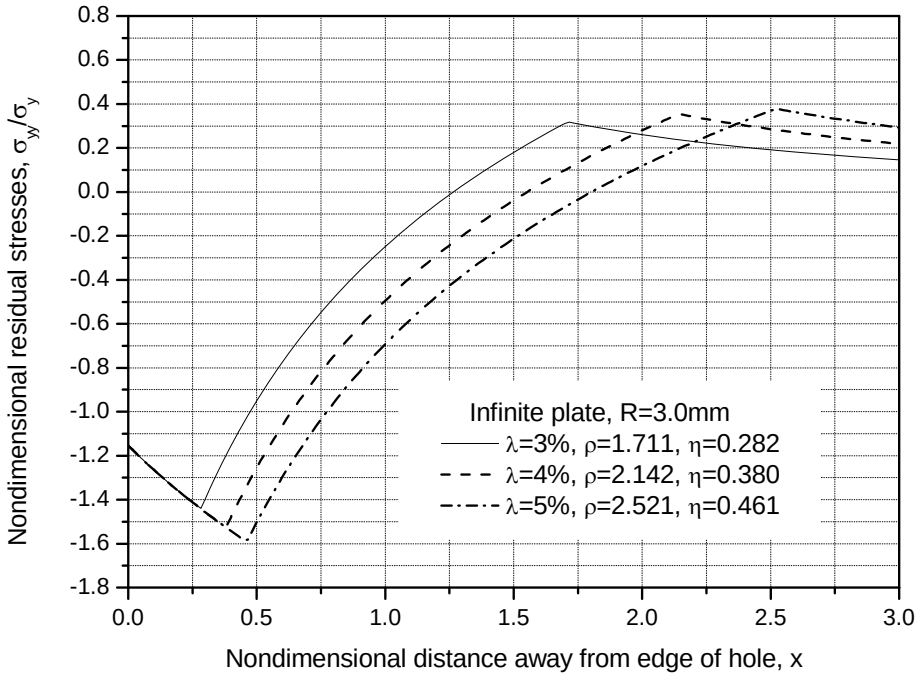

Figure 29: Residual stresses along prospective crack path due to cold expansion in a simulated infinite aluminium alloy plate with w/R = 3333

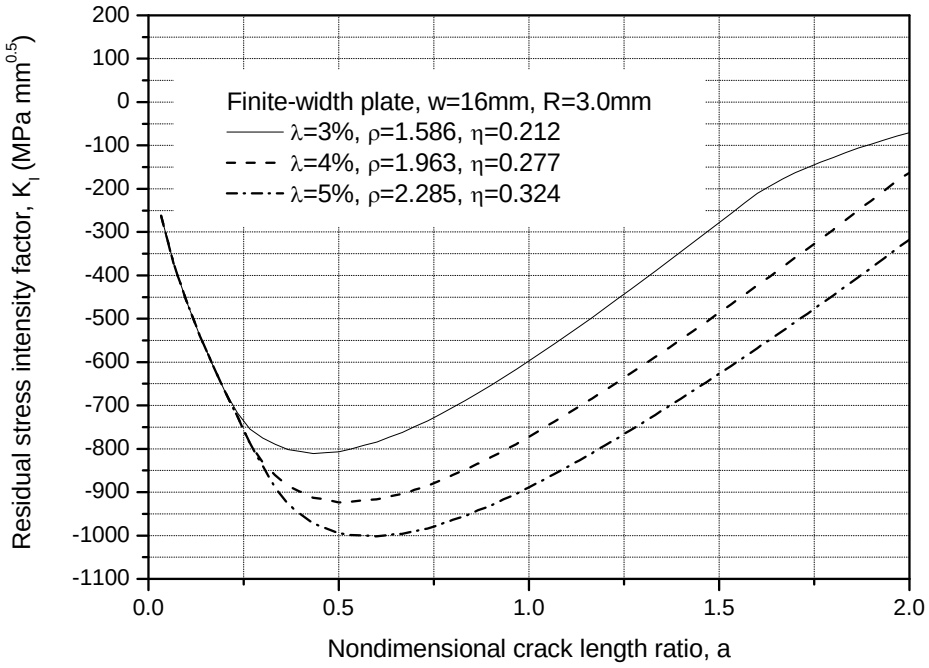

Figure 30: Residual stress intensity factor due to cold working of aluminium alloy C-130 test coupons with w/R = 5.33

Now consider a remote applied stress that is equal to the maximum spectrum tensile stress of 153 MPa. The resulting stress intensity factor due to this load is superimposed on the residual stress intensity factor and is shown in Figure 31. The beneficial effect of the higher levels of interference is obvious. The cold expansion is very effective in keeping the crack closed over a significant crack length ratio or minimising K_I as compared to the no cold-expansion case. For this remote load, based on the stresses along the prospective crack path, Figure 32 indicates that the crack length is closed for $0 < a < 0.85$ for the 5% interference case. For the 4% and 3% interference cases, the corresponding sizes are $0 < a < 0.73$ and $0 < a < 0.57$, respectively. The magnitude of the error for large cracks has not been fully investigated at this stage.

By comparing Figure 31 to Figure 22, it can be seen that, for the realistic cases considered, the cold expansion in aluminium alloys is much more effective than in D6ac steel in minimising K_I values, due to the much larger initial plastic yield zone sizes.

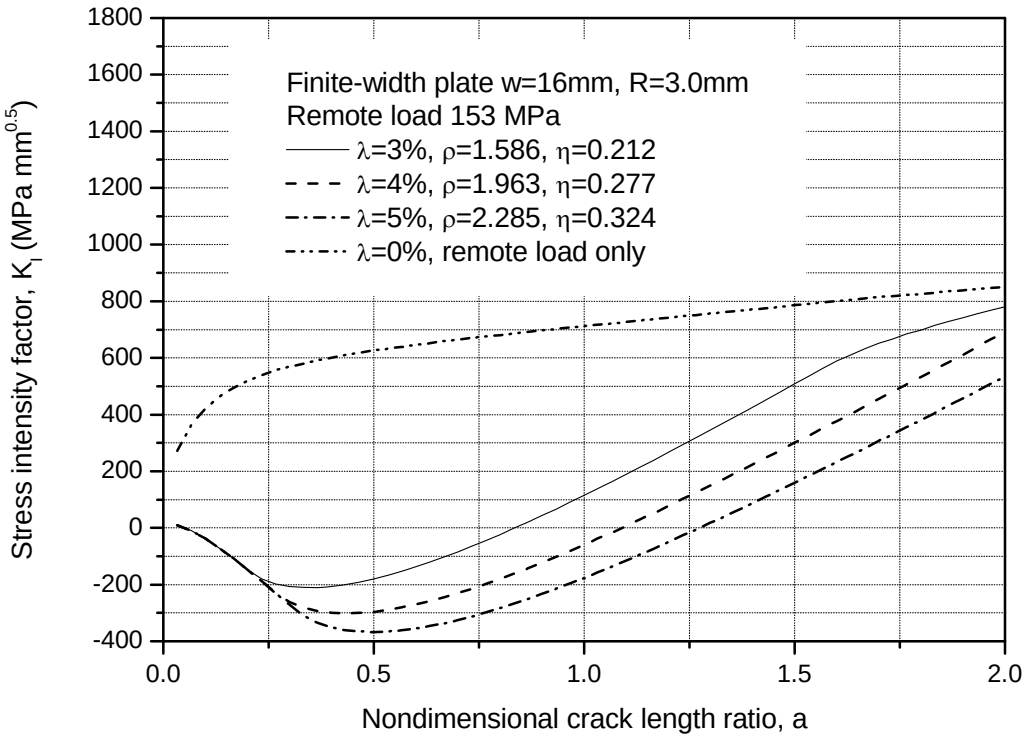

Figure 31: Stress intensity factor due to cold working of aluminium alloy C-130 fatigue test coupons with w/R = 5.33, and subsequent remote load of 153 MPa.

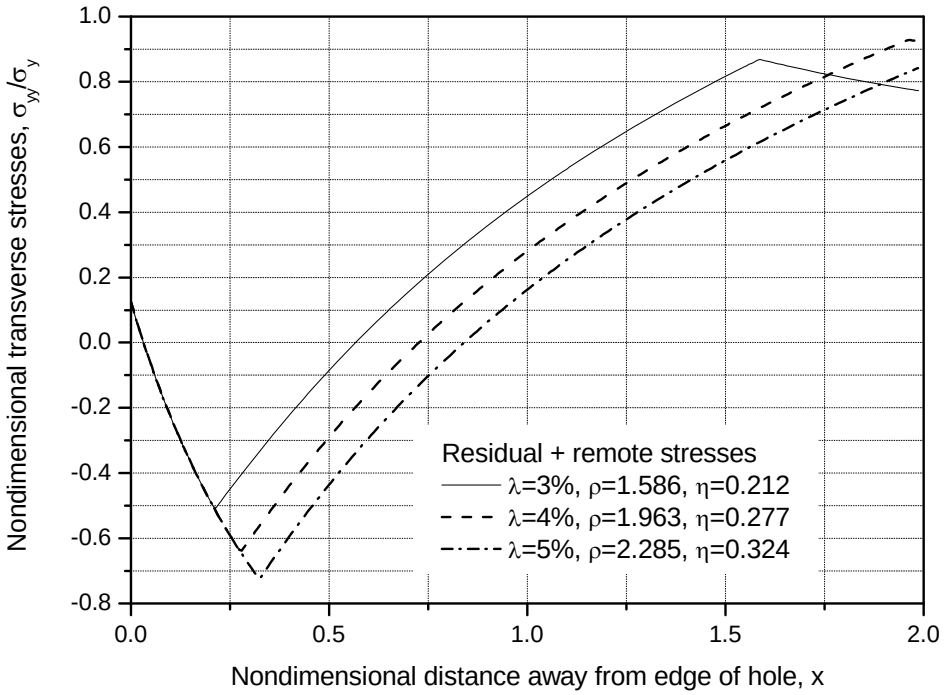

Figure 32: Transverse stresses along prospective crack path for finite-width aluminium alloy plate with w/R = 5.33 due to cold working and subsequent remote stress of 153 MPa

6.3.1 Investigation of weight function integrand

In order to investigate crack closure effects, it is useful to explore in more detail the weight function integrand $\sigma_{yy}(x)m(x,a)$ for the case of cold working with a subsequent remote stress of 153 MPa. This is undertaken for the finite-width plate with w/R = 5.33 and three different crack lengths, i.e. 0.855 mm, 1.140 mm and 1.710 mm, for the 3% interference case. From Figure 33, it is seen that, for increasing crack lengths beyond a = 0.57, the positive values of $\sigma_{yy}(x)m(x,a)$ increase quickly and significantly. For this particular case, this behaviour suggests that the negative contribution from $\sigma_{yy}(x)m(x,a)$ in the range to $0.03 \le x \le 0.57$, due to the negative values of $\sigma_{yy}(x)$ in that region, can be ignored for large cracks.

Hence, in order to better account for partial crack closure when using the weight function method, with the said partial crack closure being caused by large negative stresses, and as a conservative approximation, the value of the combined stresses $\sigma_{yy}(x)$ is here set to zero whenever $\sigma_{yy}(x) < 0$. The results for K_I obtained on this basis are shown in Figure 34. In comparison to Figure 31, apart from the elimination of negative values of K_I, the positive values of K_I have been increased. A possible better method would be to implement the formulation of [25] to the present problem.

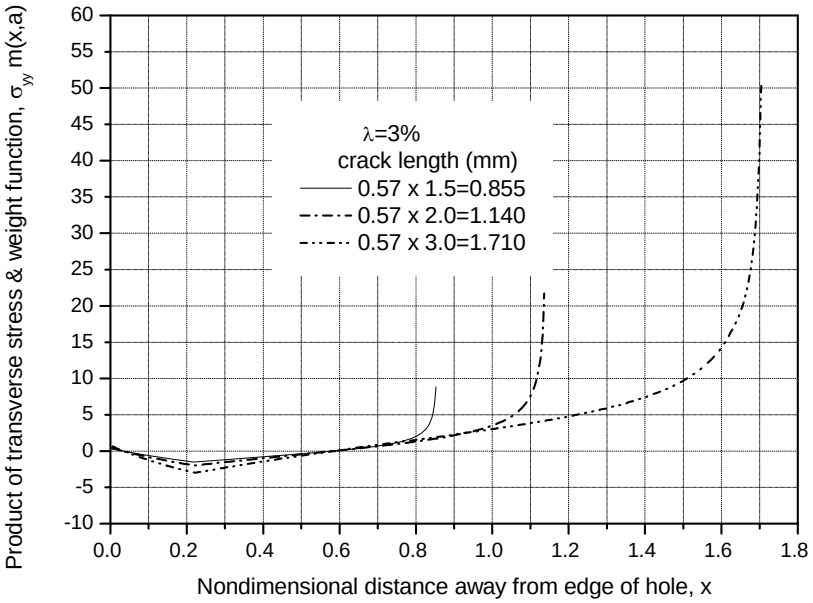

Figure 33: Evaluation of the product of the transverse stress distribution and the weight function, $\sigma_{yy}(x)m(x,a)$, as a function of distance away from the hole for various crack lengths

6.3.2 Accuracy check for finite-width correction approach

All prior sections (i.e. 4, 5, and 6.1) have considered remote loading applied to a large plate. The high accuracy of the implemented weight function approach, at least for elastic conditions, was demonstrated in Section 5.3. Here, it is useful to also check the accuracy of the weight function method when applied to a finite-width plate, for the remote-load-only case of 153 MPa tension, under elastic conditions. A standard solution for K_I can be found in Rooke and Cartwright [33, Figure 105], corresponding to two cracks at a circular hole in a rectangular sheet (sheet height equal to twice the sheet width) subjected to a uniform uniaxial tensile stress. The data are quoted to be accurate to within 1% and are comprised of three curves, corresponding to values of w/R of 2, 4, and ∞, which were created from tabulated values published by Newman [34].

Approximate solutions for the present case with w/R = 5.33 for nondimensional crack length ratios of a = 0.5, 1.0, and 1.5 were obtained from [33] by interpolation. The comparison of the results thus obtained with the weight function computations is given in Figure 34, where it can be seen that there is good agreement for the small crack size of a = 0.5. However, for crack lengths that are longer than a = 0.5, an increasingly large discrepancy is evident, indicating that K_I is here being underestimated. This can be expected, because the weight function used here is applicable to cracks in large plates, but has been utilised here in conjunction with the stresses associated with a finite-width plate. Hence, the error due to this approximation increases as the crack size increases. It should be noted that this error would apply linearly to each of the interference level cases, and the relative trends would be unchanged.

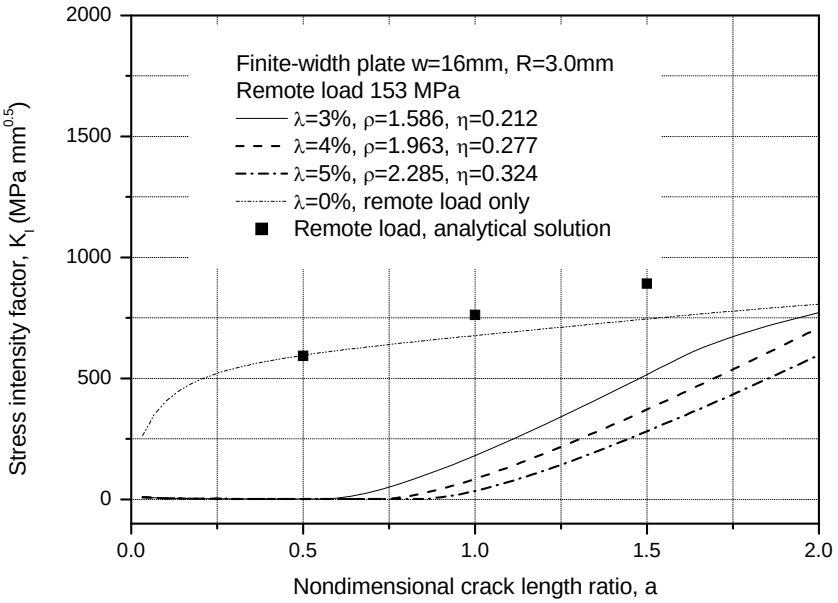

Figure 34: Stress intensity factor due to cold working of aluminium alloy C-130 test coupons with w/R = 5.33 and subsequent remote load of 153 MPa and where $\sigma_{yy}(x) = 0$ *for* $\sigma_{yy} < 0$

7. Tensile overload case – weight function approach

Consider the case of a tension overload on a large D6ac steel plate containing a 5 mm radius hole for the case of plane stress. Overloads of $0.5\sigma_Y$, $0.45\sigma_Y$ and $0.4\sigma_Y$ followed by unloading are investigated. These load levels are sufficient to result in initial plastic yield zone sizes of ρ = 0.3, 0.2 and 0.1 respectively, as indicated in Figure 10.

7.1 Residual stress field for uncracked case

The residual stress field has been determined for a tension overload followed by an unload for three different initial plastic yield zone sizes using the FEA method from Section 4. The normalised transverse residual stresses along the prospective crack path are shown in Figure 35, and indicate that a residual compressive stress is left within the initial plastic yield zone. Note that no re-yielding has occurred on the hole surface during unloading. The corresponding normalised radial stresses are plotted in Figure 36, and these are of significantly lower magnitude than the transverse stresses.

For the prospective crack path, the total stress due to residual stress and a remote stress of 200 MPa is shown in Figure 37. For the cases with ρ = 0.1 and 0.2, the crack is always open for the combined condition ($\sigma_{yy} / \sigma_y > 0$). Also, it can be seen in Figure 37 that for ρ = 0.3 there will be crack closure for $0 \le x \le 0.031$, because $\sigma_{yy} / \sigma_y \le 0$ in this region. Hence, K_I, which is

calculated assuming a fully-opened crack, is not valid in this range. For cracks of length $x > 0.031$ there is some error, which reduces with increasing crack length. In order to investigate this further, FEA has been used in Figure 38 to plot the percentage of crack opening versus nondimensional crack length, a, for the case of a remote load of 200 MPa and $\rho = 0.3$. This shows that, up till crack lengths of $a = 0.07$, the crack is fully closed, and for crack lengths of $a > 0.1$ the crack is fully open. This means that the weight function method will be accurate for predictions of stress intensity for $a > 0.1$, and for $a < 0.07$ the value of K_I will be zero. Furthermore, it has been calculated using FEA that for remote stresses of 200 MPa the crack is fully open. Of less interest is the 180 MPa case for $\rho = 0.3$, which is shown in Figure 38, which was only considered in order to investigate the sensitivity of crack closure to remote stress level.

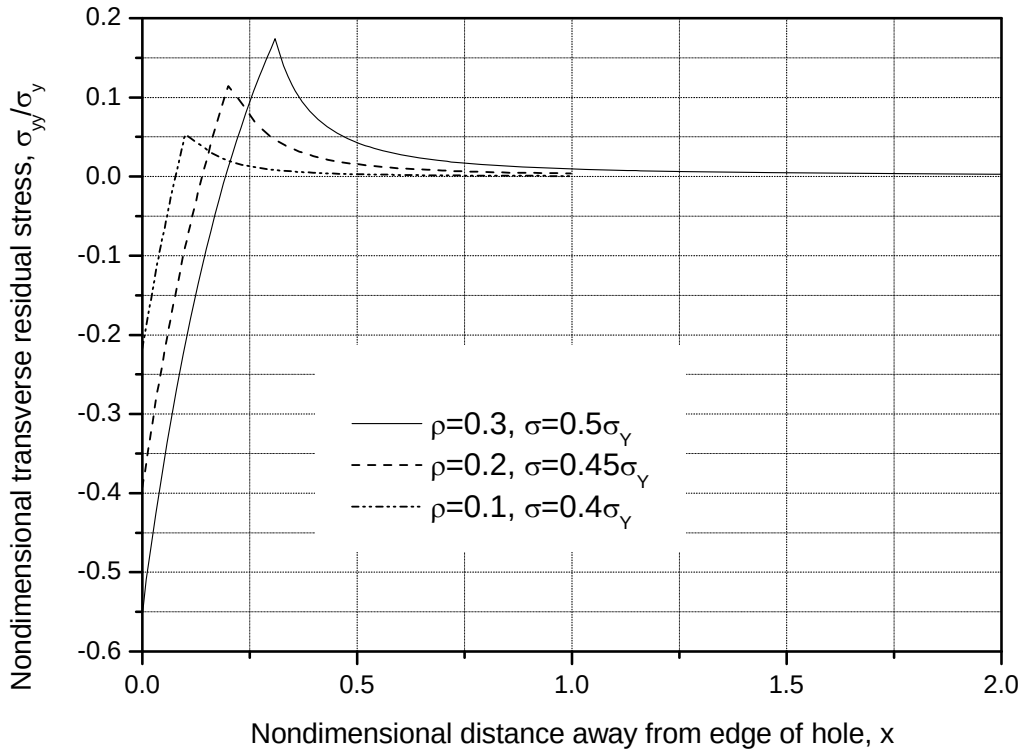

Figure 35: Transverse residual stresses along prospective crack path for a large D6ac steel plate, due to remote tensile overload followed by unload

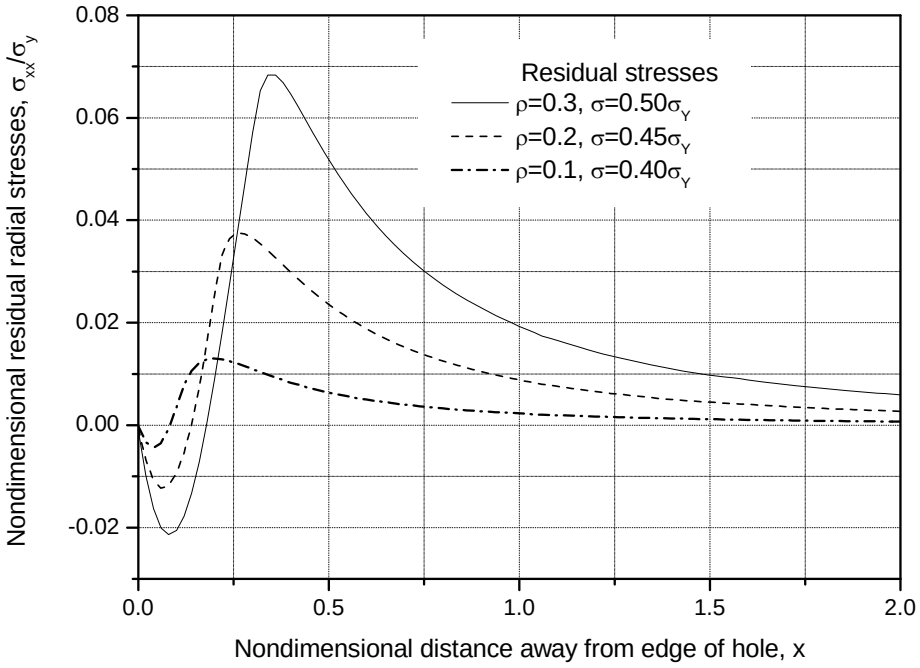

Figure 36: Residual radial stresses along prospective crack path for a large D6ac steel plate, due to remote tensile overload followed by unload

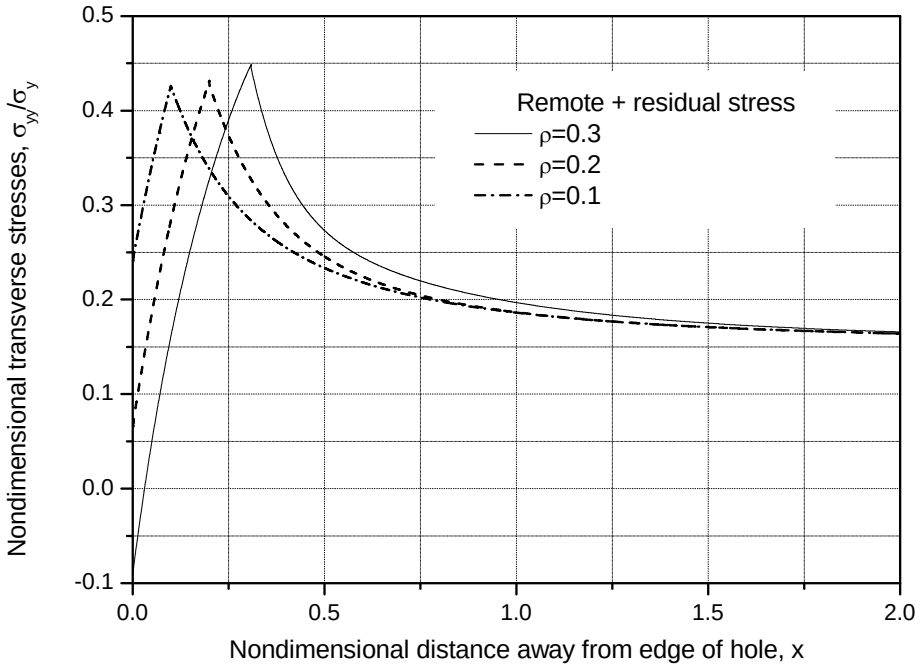

Figure 37: Transverse stresses along prospective crack path for a large D6ac steel plate; total stress due to subsequent remote load of 200 MPa

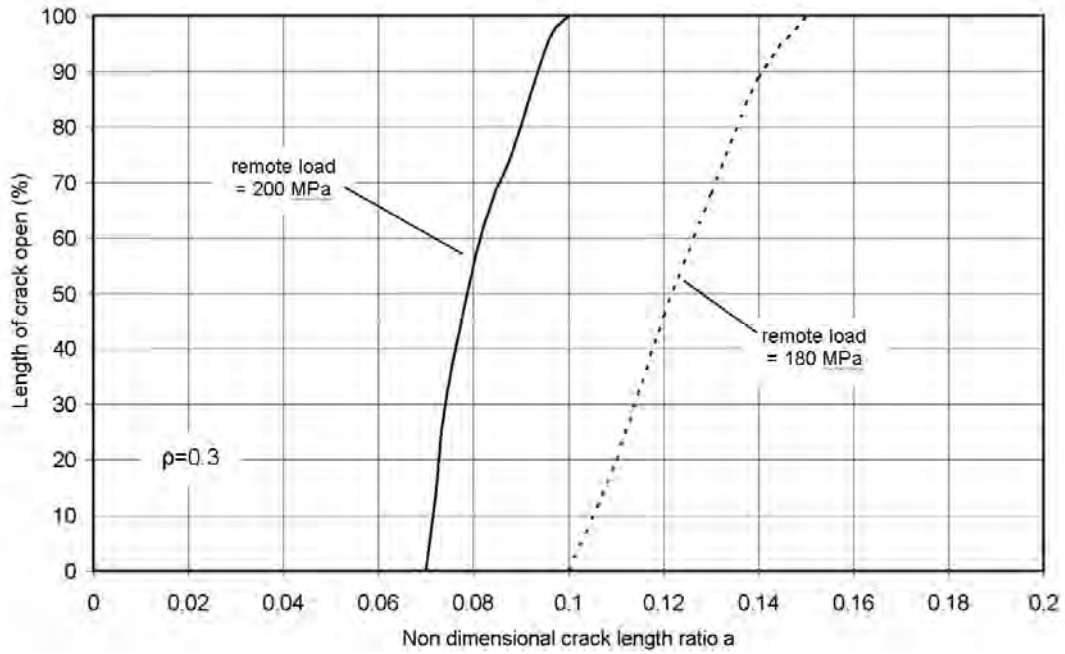

Figure 38: Length of crack opening versus nondimensional crack length ratio, a, for remote load of 200 MPa and 180 MPa, where $\rho = 0.3$

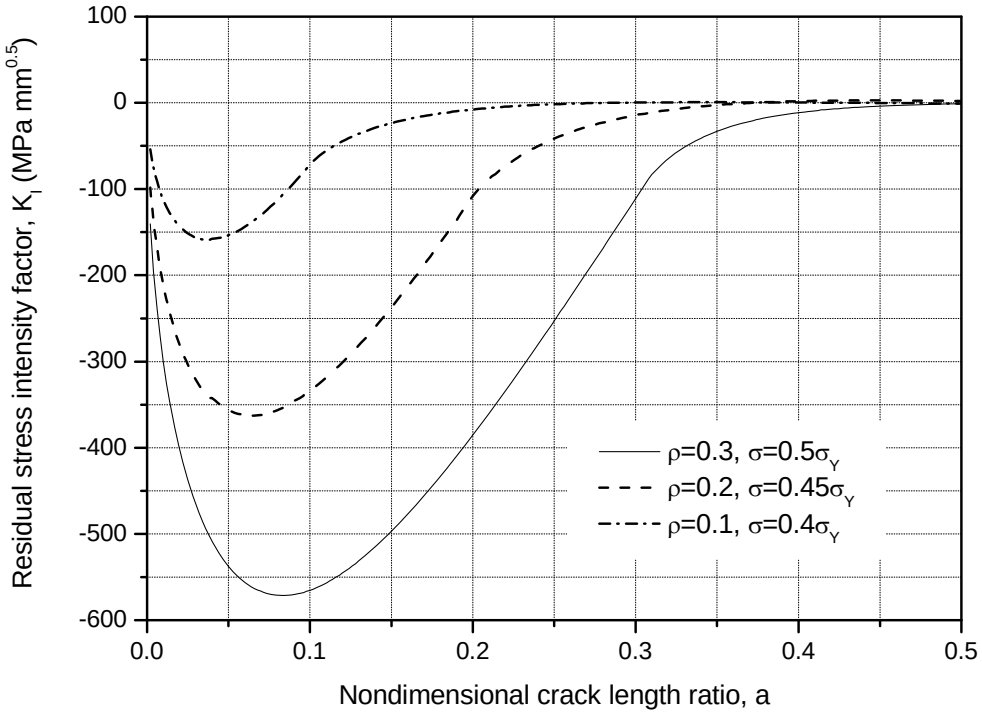

Figure 39: Stress intensity factor for a large D6ac steel plate following tension overload and unload

7.2 Stress intensity factor due to residual stress field

Using the weight function technique, from Equation (2), the residual stress intensity factors are determined for nondimensional plastic zone sizes corresponding to ρ = 0.1, 0.2 and 0.3. The residual stress intensity versus crack length ratio is given in Figure 39, and for ρ = 0.3 it shows a peak negative stress intensity of 569 MPa mm$^{0.5}$ at a crack length ratio of a = 0.09. Smaller initial yield zone sizes show a reduced peak negative stress intensity factor and the peak occurs at a lower crack length ratio.

7.3 Stress intensity factor due to overload and subsequent remote loading

Stress intensity factor results are given here for the combined case of overload-induced residual stress with the addition of a remote tensile load of 200 MPa, as shown in Figure 40. Once again, nondimensional plastic zone sizes of ρ = 0.1, 0.2 and 0.3 have been considered. When ρ = 0.3, the edge of the yielded zone extends out to a = 0.30. For comparison purposes, the results for the case of the remote tensile load alone are also given. The beneficial effects of the residual stresses due to the overloading are clearly evident when the crack is relatively small. However, once the crack has grown through the initial yield zone the beneficial effect is eliminated. As expected, greater beneficial effects are apparent for the larger initial plastic zone sizes. As a check on the accuracy of the present approach, results for the case of remote stress only are compared to a linear-elastic analytical solution taken from Bowie [35]. The comparison is given in Figure 40 where very good agreement is shown for the remote load only case.

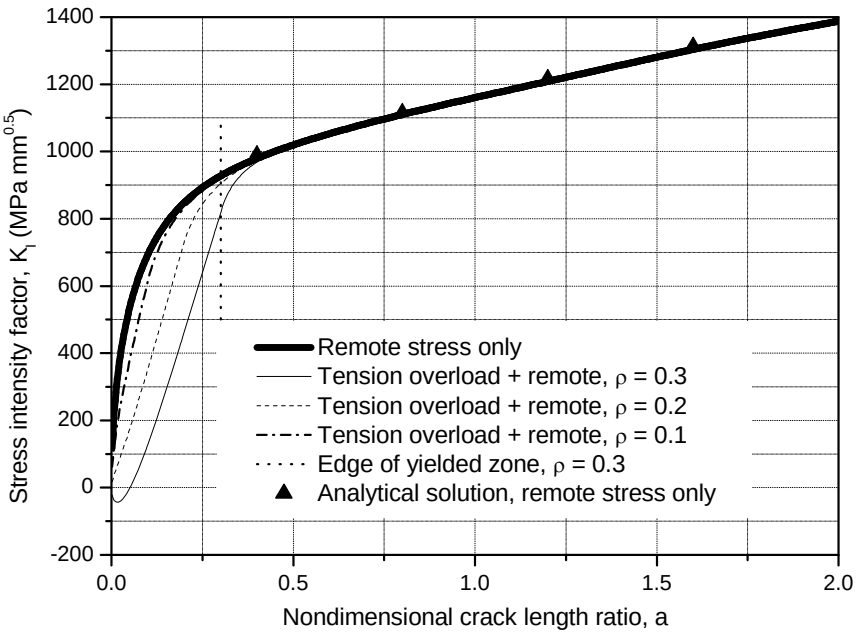

Figure 40: Stress intensity factor results due to remote overload for a large D6ac steel plate with subsequent remote load of 200 MPa

8. Compression overload case – weight function approach

In this section, we consider a large remotely-loaded D6ac steel plate with a central hole (see Figure 1). Initially, the residual stress field is determined by FEA, for the uncracked case for 2 levels of initial plastic yield zone size, due to a remote compressive overload. Then the corresponding stress intensity factor results are given. Finally, the stress intensity factor is determined with a subsequent remote tensile service load of 200 MPa.

8.1 Residual stress field for uncracked case

The normalised transverse residual stresses, σ_{yy} / σ_y, along the prospective crack path have been computed for two values of nondimensional plastic zone size, ρ = 0.2 and 0.3, and are shown in Figure 41. In this instance, it is apparent that the compression overload has left residual tensile stresses within the initial plastic yield zone. As expected, they are the same magnitude but of opposite sign to those given in Figure 35 for the tensile overload case.

8.2 Stress intensity factor due to residual stress field

From the residual stress data in Figure 41, Equation (2) has been used to generate the stress intensity factor as a function of nondimensional crack length ratio, a, and the results are shown in Figure 42. Here the maximum residual value of K_I is 559 MPa mm$^{0.5}$ for ρ = 0.3 and 359 MPa mm$^{0.5}$ for ρ = 0.2.

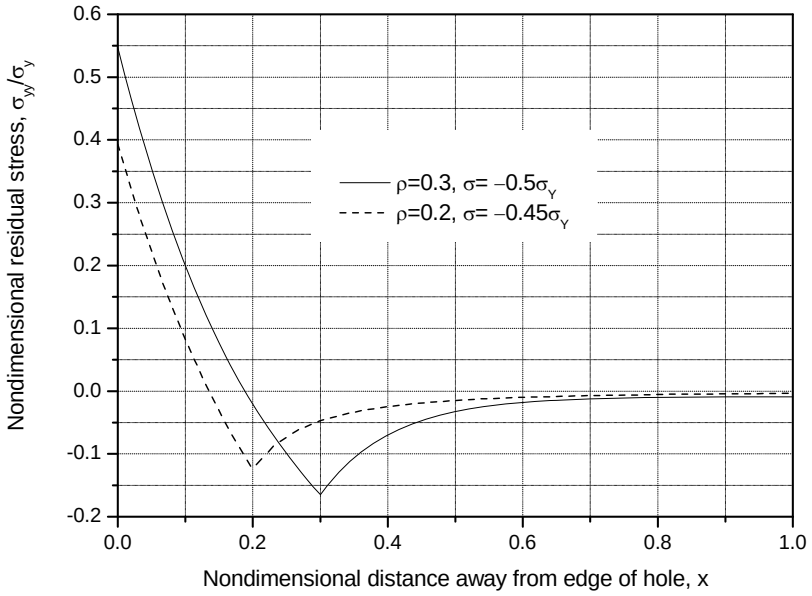

Figure 41: Stresses along prospective crack path for a large D6ac steel plate, residual stresses due to compressive overload followed by unload

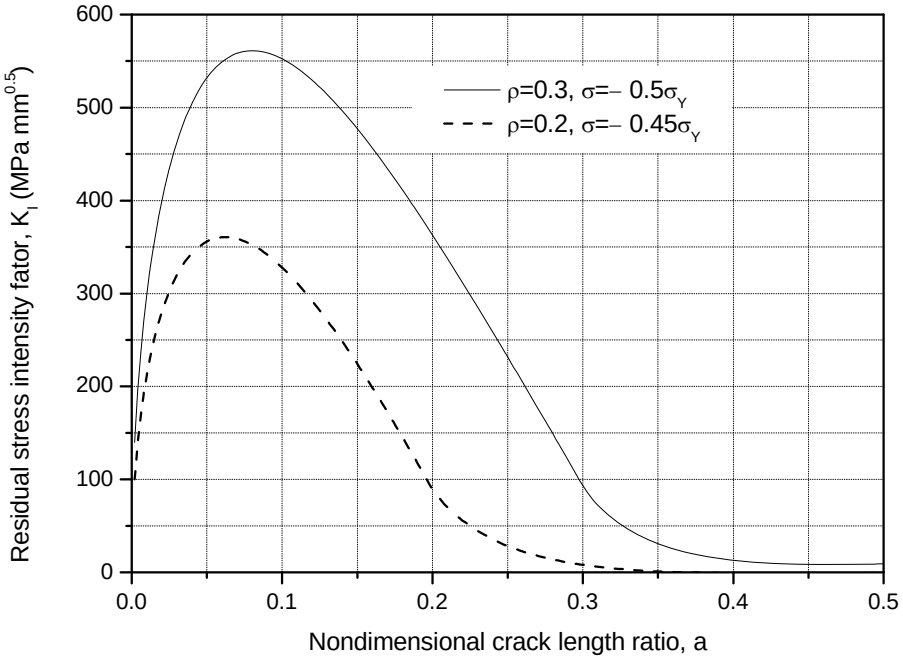

Figure 42: Stress intensity factor results due to remote compression overload for a large D6ac steel plate followed by unload

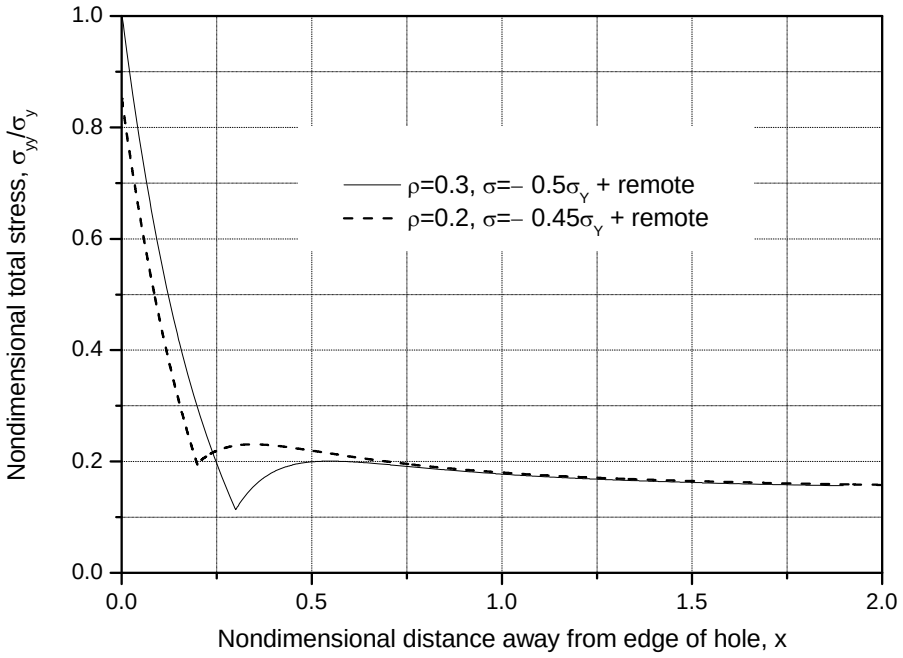

Figure 43: Total stresses along prospective crack path for a large D6ac steel plate due to remote compression overload followed by unload and then subsequent remote tensile stress of 200 MPa

8.3 Stress intensity factor due to overload and subsequent remote loading

The total stress due to the overload-induced residual stress and a remote stress of 200 MPa is shown in Figure 43 for the uncracked body. As expected, it can be seen that a prospective crack would be open at all times and the weight function method will be valid for all crack lengths. The corresponding stress intensity factors are shown in Figure 44. Here the maximum K_I of 1279 MPa mm$^{0.5}$ occurs at a crack length ratio of a = 0.14, i.e. 0.7 mm, for an initial yield zone size of ρ = 0.3. For ρ = 0.2, the maximum K_I is 1022 MPa mm$^{0.5}$ and occurs at a crack length ratio of a = 0.12, i.e. 0.6 mm. However, when the growing crack extends beyond the initial yield zone, K_I reduces significantly and closely follows the curve for the case of no residual tensile stress but with remote loading only.

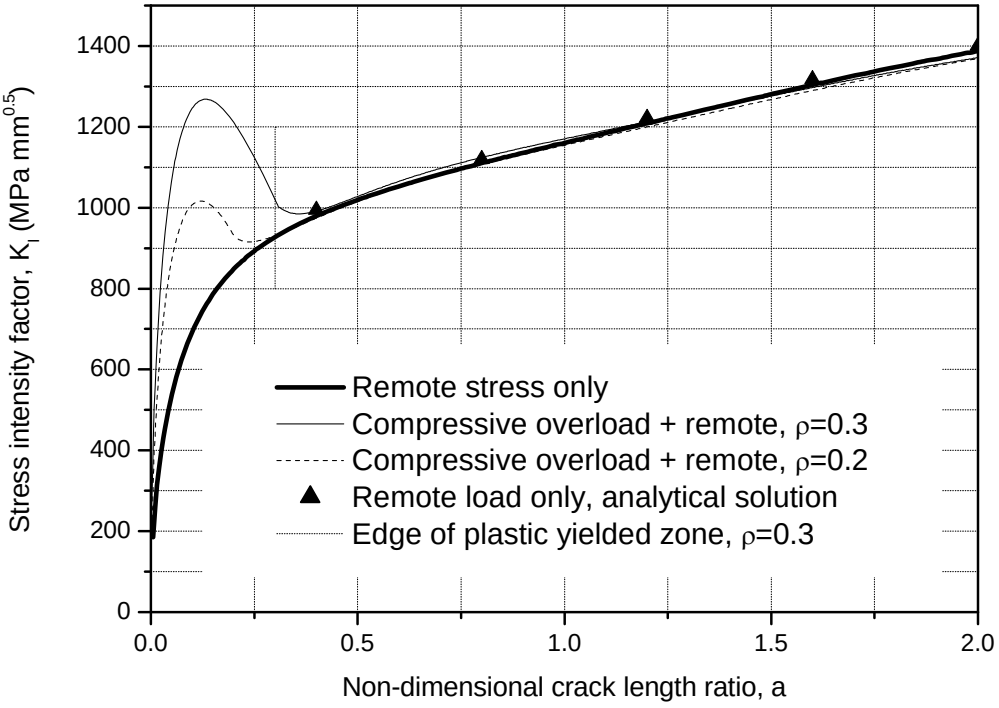

Figure 44: Stress intensity factor results due to remote compression overload for a large D6ac steel plate with subsequent remote stress of 200 MPa

9. Comparison of tension overload and cold expansion

In this section, initially comparison is made between plane stress and plane strain results obtained for the tension overload case for a large D6ac steel plate. Then comparison between cold expansion and tension overload for the same plastic zone size is made, again for the case of a large D6ac steel plate. Furthermore, a comparison is made between a tension-overloaded and cold-expanded hole in a large aluminium plate for the case of plane strain.

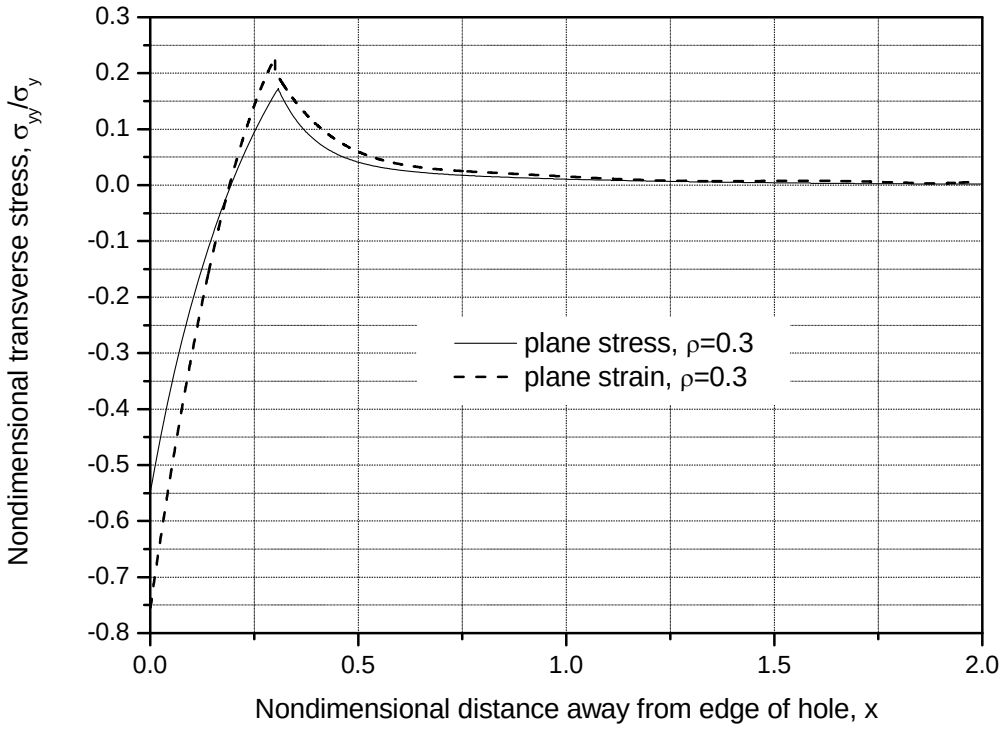

Figure 45: Comparison of transverse stresses σ_{YY}/σ_Y for plane stress and plane strain for tension overload followed by unload in a large D6ac steel plate

9.1 Comparison of stress intensity factors for plane stress and plane strain

Most of the overload cases reported up to this stage have been undertaken assuming plane stress while the equations for cold expansion correspond to the case of plane strain. Hence, it is useful to first make a comparison between plane stress and plane strain on the basis of the same plastic zone size, ρ, for D6ac steel, both with a tension overload, as shown in Figure 45. It can be seen that the plane-strain case results in slightly higher positive peak values and also higher negative peak values at the same ρ value.

The computed residual stress intensity factor due to the overload is shown in Figure 46 under conditions of plane stress and plane strain with the same plastic zone size. The residual stress intensity factor displays a considerably greater peak negative value for plane strain, being –808 MPa $mm^{0.5}$, compared with –571 MPa $mm^{0.5}$ for the case of plane stress.

Consider now the stress intensity factor subject to a service load of 200 MPa, as shown in Figure 47. Except for very small crack lengths, the disagreement is small. However, the overload that is required to produce the specified plastic zone size is significantly different, being $\sigma = 0.5\sigma_y$ for plane stress and $\sigma = 0.622\sigma_y$ for plane strain. This is expected because the von Mises stress yield condition depends on the triaxial stress field.

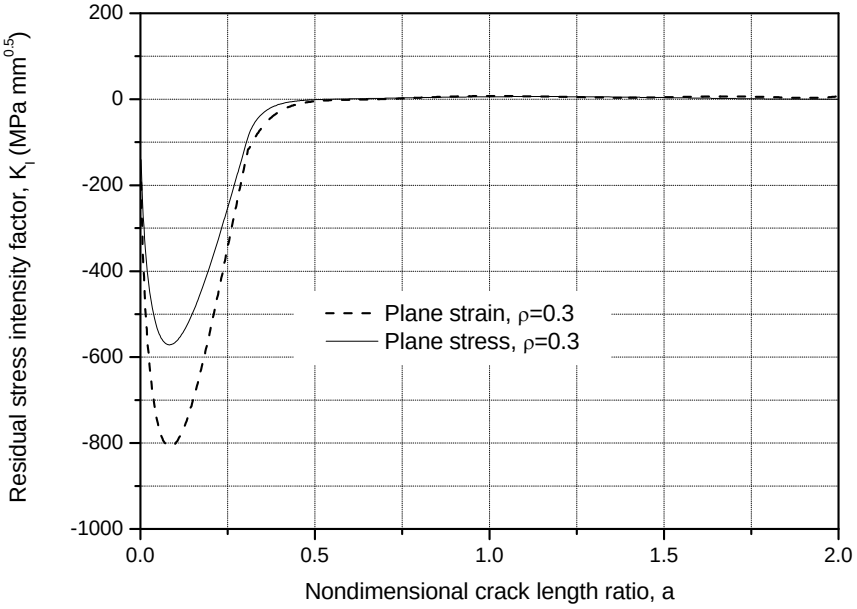

Figure 46: Comparison of K_I for plane stress and plane strain for tension overload in a large D6ac steel plate

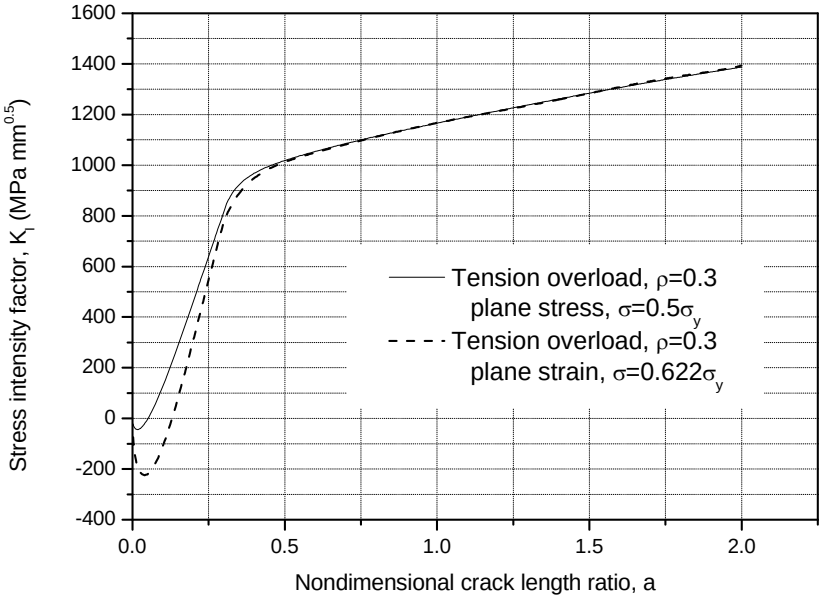

Figure 47: For tension overload a comparison of K_I for plane stress and plane strain for the same initial plastic yield zone size in a large D6ac steel plate, subject to service load of 200 MPa

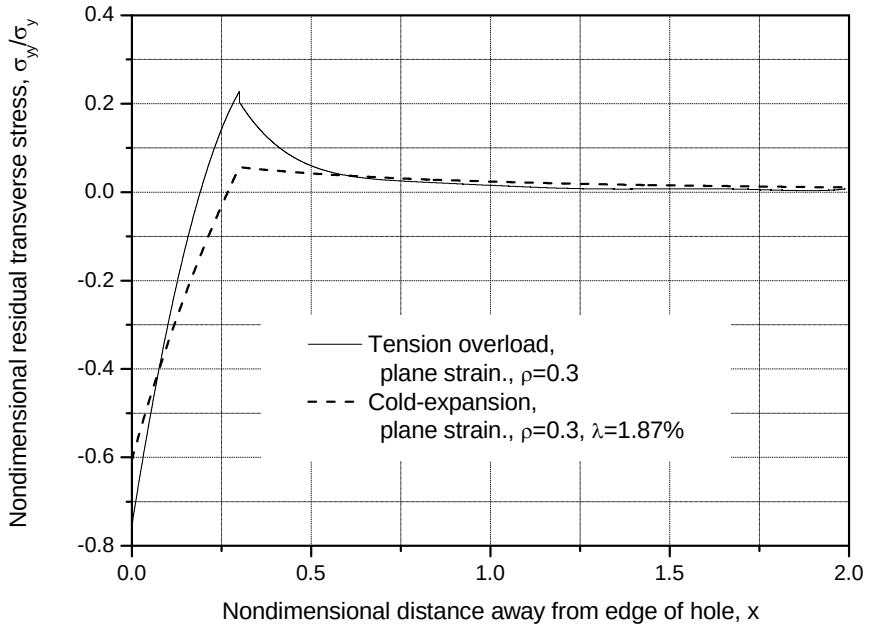

Figure 48: Comparison of stresses along prospective crack path for tension overload and cold-worked hole subsequent to remote load in a large D6ac steel plate, assuming plane strain

9.2 Comparison of results for cold expansion and tension overload

It is useful to compare the results obtained from cold expansion with those from tension overload, since they both result in residual compressive stresses at the hole edge. However, all the overload cases presented in the previous section are for plane stress conditions, while the equations for cold expansion were derived for the case of plane strain.

9.2.1 Steel plate example

To allow comparison, the previous FEA is repeated for the tension-overload case but this time using plane strain conditions in a large plate with a hole of radius R = 5 mm. The amplitude of the remote tension load is chosen so that the plastic zone size is ρ = 0.3. The comparison of the residual transverse stress results is given in Figure 48 for D6ac steel. This shows that the tension-overload case has a much higher positive peak stress than the cold-expansion case. The peak negative stress value is also larger for the tension-overload case. The residual stress intensity factor is shown in Figure 49 and indicates that for short cracks (i.e. for values of a in the range 0.05–0.13) the tension overload is more effective. However, the cold-expanded hole is significantly more effective away from the edge of the hole.

These differences are expected to be due to the fact that the cold working affects the entire circumference of the hole, while the effect of the tension overload is more localised. Hence, the tension overload is only expected to be useful for relatively small cracks, as compared to the hole size. Some further minor contribution to these differences can also be expected since, for the tension-overload case, the material response has some post-yield strain hardening and the

plate width is $R/W = 10$, while for the cold-expansion case R/W approaches infinity, and the material response has no post-yield hardening.

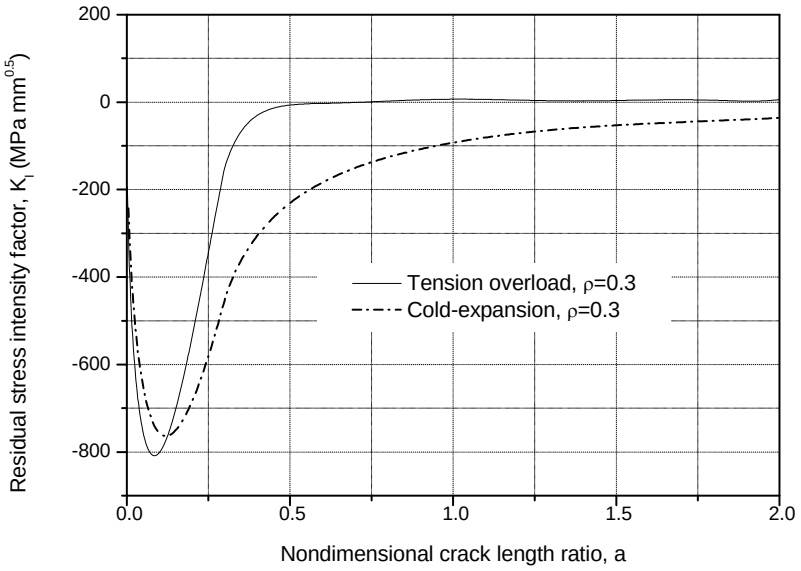

Figure 49: Comparison of residual stress intensity factor for tension-overloaded hole and cold-worked hole in a large D6ac steel plate

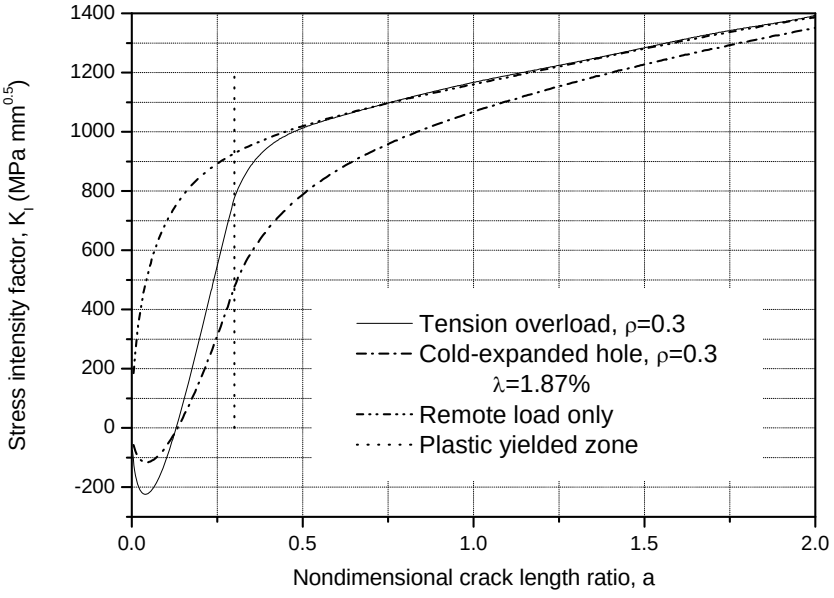

Figure 50: Comparison of stress intensity factors for a large D6ac steel plate with remote tension overload or cold-worked hole and the same subsequent remote load of 200 MPa

A comparison of results between a tension-overloaded hole case and a cold-expanded hole case, both subjected to a remote tension stress of 200 MPa, has been made in Figure 50 for D6ac steel. It can be seen that cold working is generally more effective in minimising K_I once $a > 0.14$, and has an influence beyond the initial plastic yield zone. This may be due to the fact that a cold-worked hole has plasticity induced all the way around the hole, while the tension overload produces localised plasticity only.

9.2.2 Aluminium alloy plate example

To further explore these trends, the case of an aluminium alloy plate is considered for plane strain conditions. In Figure 51 a comparison is made between a tension-overloaded (320 MPa) and cold-expanded hole (2.02%) in aluminium for $\rho = 1.193$. In both cases plane strain is assumed and a subsequent remote tension stress of 153 MPa is then applied. The cold-expanded hole is significantly more effective in reducing K_I than the overloaded hole. Note also that there is a local increase in the overload curve at a crack length ratio of $a = 0.15$; this is due to re-yielding at a distance corresponding to a nondimensional re-yield radius of $\eta \approx 0.15$.

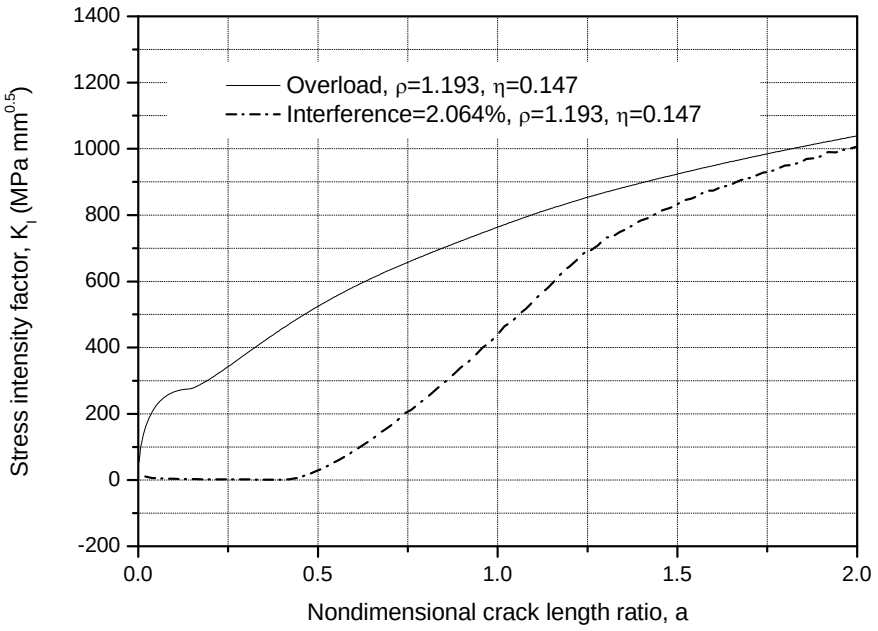

Figure 51: Comparison of stress intensity factors for a large aluminium alloy plate with remote tension overload or cold-worked hole and the same subsequent remote load of 153 MPa, for plane strain

10. Conclusions

A weight function approach has been used to determine stress intensity factors for cracks at holes in metallic plates, in the presence of either compressive or tensile residual stress fields, caused by three types of overloads, and with and without the subsequent application of remote loading. The overload types are remote tension, remote compression and hole cold expansion. Many numerical cases are considered to investigate the key trends in stress intensity factor.

Some points to note are as follows:

(i) All stress results in the corresponding uncracked body are presented in nondimensional terms normalised to the yield stress, so there is some transferability of the results.

(ii) Cold expansion of both steel and aluminium plates for realistic interference levels was investigated. It was found that, for the same plastic zone size, cold expansion is more effective in reducing the stress intensity factor than remote tensile overload.

(iii) For realistic cold-expansion levels, a much larger plastic zone size was achieved by cold expansion of a hole in an aluminium alloy plate as compared to a D6ac steel plate, resulting in an increased relative benefit in reducing the stress intensity factor.

(iv) For all overload cases, for cracks in the initial yield zone a greater effect on stress intensity factor occurred for larger magnitudes of the overload.

(v) For both remote overload cases, it was shown that, once the crack length was the same or larger than the initial yield zone size, the stress intensity factor was the same as for the case without the initial overload.

(vi) However, for the cold-expanded hole case, the beneficial reduction in stress intensity factor extended (as compared to the tensile overload) for some distance outside the initial yield zone.

(vii) The application of cold expansion to an aluminium alloy fatigue test coupon representing a lower wing skin location in the C-130 aircraft was considered. For a finite-width plate, the compressive residual stresses at the hole edge were greater in magnitude than for a large plate.

(viii) Overall the present results have been benchmarked favourably against other solutions where they are available.

(ix) For cases with local residual compressive stresses, some understanding has also been gained of the potential inaccuracies in the present formulation of the weight function method due to the presence of regions of likely crack closure. This effect reduces with increasing crack length. It is recommended that further work be undertaken to implement the method of Yu and Abel [25] to the present problem.

11. Acknowledgements

The authors would like to thank the AVD CSAF support team for providing the computing facilities necessary to do this work. Also the authors would like to thank Mr Witold Waldman for reviewing the manuscript.

12. References

1. HF Bueckner. *A novel principle for the computation of stress intensity factors*. Zeitschrift für Angewandte Mathematik und Mechanik (ZAMM), Vol 50, No 9, pp 529–546, 1970.

2. J Rice. *Some remarks on elastic crack-tip stress fields*. International Journal of Solids and Structures, Vol 8, Issue 6, pp 751–758, 1972.

3. XR Wu and AJ Carlsson. *Weight functions and stress intensity factor solutions*. First edition, Pergamon Press, 1991.

4. A Kiciak, G Glinka and M Eman. *Weight functions and stress intensity factors for corner quarter-elliptical crack in finite thickness plate subjected to in-plane loading*. Engineering Fracture Mechanics, Vol 60, No 2, pp 221–238, 1998.

5. Q Chen and X Wang. *Weight functions and stress intensity factors for quarter-elliptical corner cracks in fastener holes*. Fatigue & Fracture of Engineering Materials & Structures, Vol 27, Issue 8, pp 701–712, 2004.

6. G Glinka and G Shen. *Universal features of weight functions for cracks in Mode I*. Engineering Fracture Mechanics, Vol 40, No 6, pp 1135–1146, 1991.

7. T Mawatari, DV Nelson. *Method for efficient computation of stress intensity factors from weight functions by singular point elimination*. Engineering Fracture Mechanics, Vol 78, Issue 18, pp 2713–2730, Nov 2011.

8. SR Daniewicz. *Accurate and efficient numerical integration of weight functions using Gauss-Chebyshev quadrature*. Engineering Fracture Mechanics, Vol 48, Issue 4, pp 541–544, July 1994.

9. AF Grandt and TE Kullgren. *Tabulated stress intensity factor solutions for flawed fastener holes*. Engineering Fracture Mechanics, Vol 18, No 2, pp 435–451, 1983.

10. PC Paris, RM McMeeking and H Tada. *The weight function method for determining stress intensity*. Cracks and Fracture, ASTM STP 601, pp 471–489, 1976.

11. G Shen and G Glinka. *Weight functions for a surface semi-elliptical crack in a finite thickness plate*. Theoretical and Applied Fracture Mechanics, Vol 15, Issue 3, pp 247–255, 1991.

12. HJ Petroski and JD Achenbach. *Computation of the weight function from a stress intensity factor*. Engineering Fracture Mechanics, Vol 10, Issue 2, pp 257–266, 1978.

13. K Sobczyk and J Trębicki. *Fatigue crack growth in random residual stresses*. International Journal of Fatigue, Vol 26, Issue 11, pp 1179–1187, 2004.

14. R Jones, D Peng, S Pitt and C Wallbrink. *Weight functions, CTOD, and related solutions for cracks at notches*. Engineering Failure Analysis, Vol 11, Issue 1, pp 79–114, 2004.

15. W Zhao and XR Wu. *Stress intensity factor evaluation by weight function for surface crack in edge notch*. Theoretical and Applied Fracture Mechanics, Vol 13, Issue 3, pp 225–238, 1990.

16. A Roy and TK Saha. *Weight function for an elliptic crack in an infinite medium. I. Normal loading*. International Journal of Fracture, Vol 103, No 3, pp 227–241, 2000.

17. ST Pinho, HB Martins, PP Camanho, MH Santare and PMST de Castro. *Residual stress field and reduction of stress intensity factors in cold-worked holes*. Theoretical and Applied Fracture Mechanics, Vol 44, Issue 2, pp 168–177, 2005.

18. G Clark. *Modelling residual stresses and fatigue crack growth at cold expanded fastener holes*. Fatigue & Fracture of Engineering Materials & Structures, Vol 14, No 5, pp 579–589, 1991

19. MJ Pavier, CGC Poussard and DJ Smith. *Effect of residual stress around cold worked holes on fracture under superimposed mechanical load*. Engineering Fracture Mechanics, Vol 63, Issue 6, pp 751–773, 1999.

20. PMGP Moreira, PFP de Matos, ST Pinho, SD Pastrama, PP Camanho and PMST de Castro. *The residual stress intensity factors for cold-worked cracked holes: a technical note*. Fatigue & Fracture of Engineering Materials & Structures, Vol 27, Issue 9, pp 879–886, 2004. Erratum, Fatigue & Fracture of Engineering Materials & Structures, Vol 30, Issue 2, p 170, 2007.

21. Y Prawoto. *Linear elastic fracture mechanics analysis of the effect of residual stress on fatigue crack propagation rate*. PFANF8, Journal of Failure Analysis and Prevention Vol 2, Issue 5, pp 75–83, 2002.

22. MA Wahab, GR Rohrsheim and JH Park. *Experimental study on the influence of overload induced residual stress field on fatigue crack growth in aluminium alloy*. Journal of Materials Processing Technology, Vol 153–154, pp 945–951, 2004.

23. GS Wang. *A strip yield analysis of fatigue crack growth in the residual stress field*. International Journal of Fracture, Vol 96, pp 247–277, 1999.

24. JE LaRue and SR Daniewicz. *Predicting the effect of residual stress on fatigue crack growth*. International Journal of Fatigue, Vol 29, Issue 3, pp 508–515, 2007.

25. X Yu and A Abel. *Fatigue crack growth in residual stress field: implications of partial closure*. ACAM99, Canberra, Australia, 10–12 February, 1999.

26. US Department of Transport, Federal Aviation Administration, Metallic Materials Properties Development and Standardisation*, DOT/FAA/AR-MMPDS-01, January 1993.*

27. AA Moftakhar and G Glinka. *Calculation of stress intensity factors by efficient integration of weight functions*. Engineering Fracture Mechanics, Vol 43, No 5, pp 749–756, 1992.

28. SP Timoshenko and JN Goodier. *Theory of Elasticity*, Third edition, McGraw-Hill, 1970.

29. GS Jost. *Stresses and strains in a cold-worked annulus*. Aircraft Structures Report 434, AR-005-548, Defence Science and Technology Organisation, September 1988.

30. DL Rich and LF Impellizzeri. *Fatigue analysis of cold-worked and interference fit fastener holes*. Cyclic Stress-Strain and Plastic Deformation Aspects of Fatigue Crack Growth, ASTM STP 637, ASTM, pp 153–175, 1977.

31. RCJ Howland. *On the stresses in the neighbourhood of a circular hole in a strip under tension*. Transactions Royal Society of London, Series A, Vol 229, pp 49–86, 1930.

32. S Houghton and S Campbell. *Beta solution development and validation C130-J*. TTCP AER TP4, 2010.

33. DP Rooke and DJ Cartwright. *Compendium of Stress Intensity Factors*. 1976.

34. JC Newman, Jr. *An improved method of collocation for the stress analysis of cracked plates with various shaped boundaries*. NASA Technical Note D-6376, August 1971.

35. OL Bowie. *Analysis of an infinite plate containing radial cracks originating at the boundary of an internal circular hole*. Journal of Mathematics and Physics, Vol 35, No 1, pp 60–71, 1956.

This page is intentionally blank.

Appendix A: List of computer programs

A set of self-contained Fortran computer programs was written to generate the data in the Figures, and these programs are contained on a Compact Disc. These programs were run on the DSTO server Shyted under Fortran 77. The names of the programs, together with the Figure numbers in whose generation they participated, are presented in Table A1. The contents of the files on Compact Disc are described in Table A2. The variables used in the computer programs are described in Table A3.

Table A1: Fortran computer programs used to generate data in the Figures

Program Number	Program Name	Name Of Main Output File	For Generation Of Data In Figure
25	wtfunc00.f	ans1	13
26	wtfunc50.f	ans	15
24	wtfun1150.f	what	17
36	wtfungj10.f	new	18
37	wtfungj11.f	new	19
38	wtfungj12.f	new	20
1	wtfun11.f	ans0	21
1	wtfun11.f	ans0	22
40	wtfungjps3.f	new	23
41	wtfungjps4.f	ans	24
39	wtfungj.f	new	25
33	wtfungj05.f	new	28
31	wtfungj01.f	new	29
32	wtfungj04.f	ans	30
32	wtfungj04.f	ans	31
34	wtfungj06.f	new	32
22	wtfun110.f	valid	33
23	wtfun111.f	ans	34
16	wtfun103.f	check	37
17	wtfun104.f	check	37
18	wtfun105.f	check	37
19	wtfun106.f	ans	39
20	wtfun107.f	ans	39
21	wtfun108.f	ans	39
19	wtfun106.f	ans	40
20	wtfun107.f	ans	40
21	wtfun108.f	ans	40
29	wtfuncx.f	ans1	42
2	wtfun33.f	ans0	42
14	wtfun101.f	check1	43
15	wtfun102.f	check2	43
30	wtfuncy.f	ans	44
27	wtfunch.f	ans	44
28	wtfunci.f	ans	44
6	wtfun78.f	check	45

Table A1 (continued): Fortran computer programs used to generate data in the Figures

Program Number	Program Name	Name Of Main Output File	For Generation Of Data In Figure
7	wtfun79.f	check1	45
9	wtfun81.f	ans6	46
8	wtfun80.f	ans5	46
4	wtfun74.f	ans8	47
5	wtfun75.f	ans0	47
10	wtfun82.f	check	48
11	wtfun83.f	check1	48
13	wtfun85.f	ans0	49
12	wtfun84.f	ans1	49
5	wtfun75.f	ans0	50
1	wtfun11.f	ans0	50
3	wtfun73.f	ans	51
42	wtfungjps5.f	ans	51
35	wtfungj07.f	ans	–

Table A2: Description of files on Compact Disc.

Program	Description	Figures
wtfunc00.f	Two symmetric cracks emanating from a hole subject to remote tensile stress. (Validation of weight function technique.)	13
wtfunc50.f	Cold-worked hole. (Validation of Wu and Carlsson derivation.)	15
wtfun1150.f	Howland plot, using Equation (29)[2], obtained from Howland [31].	17
wtfungj10.f	Cold-worked hole and subsequent remote loading. Uses Equation (9), obtained from Timoshenko and Goodier [28].	18, 19, 20, 21, 22
wtfungj04.f	Cold-worked hole and subsequent remote loading. For finite-width plate. Uses Equation (29), obtained from Howland [31]. Also has re-yielding or no re-yielding case.	28, 29, 30, 31,32
wtfun111.f	As above, except that $K_I = 0$ for $\sigma < 0$ for re-yielding analysis only.	34
wtfungj07.f	Ream after re-yield. Cold-worked hole and subsequent remote loading. For finite-width plate. Uses Equation (29), obtained from Howland [31].	
wtfun103.f	Tension overload case. Results from FEA used to generate fourth-order polynomial and exponential decay curve fit for $\rho = 0.3$. Uses Equation (9), obtained from Timoshenko and Goodier [28].	37, 39, 40
wtfun104.f	Tension overload case. Results from FEA used to generate fourth-order polynomial and exponential decay curve fit for $\rho = 0.2$. Uses Equation (9), obtained from Timoshenko and Goodier [28].	37, 39, 40
wtfun105.f	Tension overload case. Results from FEA used to generate fourth-order polynomial and exponential decay curve fit for $\rho = 0.1$. Uses Equation (9), obtained from Timoshenko and Goodier [28].	37, 39, 40
wtfuncx.f	Compression overload case. Results from FEA used to generate third-order polynomial and exponential decay curve fit for $\rho = 0.3$. Uses Equation (9), obtained from Timoshenko and Goodier [28].	42, 43, 44
wtfun33.f	Compression overload case. Results from FEA used to generate third-order polynomial and exponential decay curve fit for $\rho = 0.2$. Uses Equation (9), obtained from Timoshenko and Goodier [28].	42, 43, 44

[2] Refers to equation number as identified in present report.

Table A3: Variables used in computer programs

Variable	Description
Sig	Yield stress
Sigl	Remote applied stress
E	Young's modulus of plate
Em	Young's modulus of mandrel
v	Poisson's ratio for plate
vm	Poisson's ratio for mandrel
R	Radius of hole
rho	*Nondimensional plastic yield zone (ρ in report)
RH	*Length of yielded zone (D_{PZ} in report)
bb	Finite width (w in report)
Lamda	Interference (λ in report)

* Is calculated in cold expansion programs, but must be set in overload program.

DEFENCE SCIENCE AND TECHNOLOGY ORGANISATION
DOCUMENT CONTROL DATA

1. PRIVACY MARKING/CAVEAT (OF DOCUMENT)

2. TITLE

Investigation of Stress Intensity Factor for Overloaded Holes and Cold-Expanded Holes

3. SECURITY CLASSIFICATION (FOR UNCLASSIFIED REPORTS THAT ARE LIMITED RELEASE USE (L) NEXT TO DOCUMENT CLASSIFICATION)

Document	(U)
Title	(U)
Abstract	(U)

4. AUTHOR(S)

Richard Callinan, Robert Kaye, and Manfred Heller

5. CORPORATE AUTHOR

DSTO Defence Science and Technology Organisation
506 Lorimer St
Fishermans Bend Victoria 3207 Australia

6a. DSTO NUMBER	6b. AR NUMBER	6c. TYPE OF REPORT	7. DOCUMENT DATE
DSTO-TR-2737	AR-015-380	Technical Report	July 2012

8. FILE NUMBER	9. TASK NUMBER	10. TASK SPONSOR	11. NO. OF PAGES	12. NO. OF REFERENCES
2010/1089196	AIR 07/283	OIC-ASI-DGTA	58	36

13. DOWNGRADING/DELIMITING INSTRUCTIONS

To be reviewed three years after date of publication

14. RELEASE AUTHORITY

Chief, Air Vehicles Division

15. SECONDARY RELEASE STATEMENT OF THIS DOCUMENT

Approved for public release

OVERSEAS ENQUIRIES OUTSIDE STATED LIMITATIONS SHOULD BE REFERRED THROUGH DOCUMENT EXCHANGE, PO BOX 1500, EDINBURGH, SA 5111

16. DELIBERATE ANNOUNCEMENT

No Limitations

17. CITATION IN OTHER DOCUMENTS Yes

18. DSTO RESEARCH LIBRARY THESAURUS http://web-vic.dsto.defence.gov.au/workareas/library/resources/dsto_thesaurus.shtml

Stress intensity factors, crack growth, weight functions, finite element analysis

19. ABSTRACT

For life assessment of airframe components, it is important to understand how the residual stresses due to material yielding affect crack initiation or crack growth at holes. A key step in understanding such effects is the quantification of the Mode 1 stress intensity factor for cracks that may initiate subsequent to overloading. Here, a two-dimensional weight function approach is used to determine stress intensity factors for cracks in either tensile or compressive stress fields due to one of three mechanisms: remote tension overload, remote compression overload or hole cold expansion. The effect of subsequent remote loading is also considered. The key input is the stress distribution in the corresponding uncracked body along the prospective crack path. The key trends are investigated through many numerical examples for symmetrically-cracked holes in large steel and/or aluminium alloy plates. Cold expansion of finite-width plates representative of C-130 wing skin locations is also studied. For both remote overload cases, it is shown that, once the crack length is the same or larger than the initial yield zone, the stress intensity factors are the same as for the case without the initial overload. However, for cold-expanded holes, the beneficial reduction in stress intensity factor extends beyond the initial yield zone. Hence, the present work provides a greater depth of understanding of how typical residual stresses can affect key inputs into airframe life assessment.